









Rab11-FIP1C Is Dispensable for HIV-1 Replication in Primary CD4⁺ T Cells, but Its Role Is Cell Type Dependent in Immortalized Human T-Cell Lines

 Melissa V. Fernandez-de Céspedes,^a
 Huxley K. Hoffman,^{b*}
 Hannah Carter,^a
 Lacy M. Simons,^d
 Lwar Naing,^a
 Sherimay D. Ablan,^a
 David A. Scheiblin,^c
 Judd F. Hultquist,^d
 Schuyler B. van Engelenburg,^b
 Eric O. Freed^a

^aHIV Dynamics and Replication Program, Center for Cancer Research, National Cancer Institute, Frederick, Maryland, USA

^bBiological Sciences, University of Denver, Denver, Colorado, USA

^cOptical Microscopy and Analysis Laboratory, Cancer Research Technology Program, Frederick National Laboratory for Cancer Research, Frederick, Maryland, USA

^dDivision of Infectious Diseases, Center for Pathogen Genomics and Microbial Evolution, Havey Institute for Global Health, Northwestern University Feinberg School of Medicine, Chicago, Illinois, USA

ABSTRACT The HIV-1 envelope glycoprotein (Env) contains a long cytoplasmic tail harboring highly conserved motifs that direct Env trafficking and incorporation into virions and promote efficient virus spread. The cellular trafficking factor Rab11a family interacting protein 1C (FIP1C) has been implicated in the directed trafficking of Env to sites of viral assembly. In this study, we confirm that small interfering RNA (siRNA)-mediated depletion of FIP1C in HeLa cells modestly reduces Env incorporation into virions. To determine whether FIP1C is required for Env incorporation and HIV-1 replication in physiologically relevant cells, CRISPR-Cas9 technology was used to knock out the expression of this protein in several human T-cell lines—Jurkat E6.1, SupT1, and H9—and in primary human CD4⁺ T cells. *FIP1C* knockout caused modest reductions in Env incorporation in SupT1 cells but did not inhibit virus replication in SupT1 or Jurkat E6.1 T cells. In H9 cells, *FIP1C* knockout caused a cell density-dependent defect in virus replication. In primary CD4⁺ T cells, *FIP1C* knockout had no effect on HIV-1 replication. Furthermore, human T-cell leukemia virus type 1 (HTLV-1)-transformed cell lines that are permissive for HIV-1 replication do not express FIP1C. Mutation of an aromatic motif in the Env cytoplasmic tail (Y₇₉₅W) implicated in FIP1C-mediated Env incorporation impaired virus replication independently of FIP1C expression in SupT1, Jurkat E6.1, H9, and primary T cells. Together, these results indicate that while FIP1C may contribute to HIV-1 Env incorporation in some contexts, additional and potentially redundant host factors are likely required for Env incorporation and virus dissemination in T cells.

IMPORTANCE The incorporation of the HIV-1 envelope (Env) glycoproteins, gp120 and gp41, into virus particles is critical for virus infectivity. gp41 contains a long cytoplasmic tail that has been proposed to interact with host cell factors, including the trafficking factor Rab11a family interacting protein 1C (FIP1C). To investigate the role of FIP1C in relevant cell types—human T-cell lines and primary CD4⁺ T cells—we used CRISPR-Cas9 to knock out FIP1C expression and examined the effect on HIV-1 Env incorporation and virus replication. We observed that in two of the T-cell lines examined (Jurkat E6.1 and SupT1) and in primary CD4⁺ T cells, FIP1C knockout did not disrupt HIV-1 replication, whereas FIP1C knockout reduced Env expression and delayed replication in H9 cells. The results indicate that while FIP1C may contribute to Env incorporation in some cell lines, it is not an essential factor for efficient HIV-1 replication in primary CD4⁺ T cells.

KEYWORDS HIV-1, Env, gp41, cytoplasmic tail, transmission, FIP1C, trafficking, incorporation, virus assembly, protein trafficking, Rab proteins, retrovirus

Editor Viviana Simon, Icahn School of Medicine at Mount Sinai

Copyright © 2022 American Society for Microbiology. All Rights Reserved.

Address correspondence to Eric O. Freed, efreed@mail.nih.gov.

*Present address: Huxley K. Hoffman, Department of Cell and Developmental Biology, University of Colorado Anschutz Medical Campus, Aurora, Colorado, USA. The authors declare no conflict of interest.

Received 2 June 2022

Accepted 11 October 2022

Published 10 November 2022

Human immunodeficiency virus type 1 (HIV-1) particle assembly takes place predominantly on the plasma membranes of infected host cells in a series of steps driven by the viral Gag polyprotein precursor. Although expression of Gag is sufficient for the formation of noninfectious virus-like particles (VLPs), the production of infectious virions requires expression and incorporation of the viral envelope glycoprotein (Env). HIV-1 Env is synthesized as a 160-kDa polyprotein precursor, gp160, on endoplasmic reticulum (ER)-associated ribosomes and is transported to the plasma membrane through the secretory pathway. During transport, gp160 trimerizes and is cleaved in the Golgi apparatus by host furin or furin-like enzymes to form two mature Env subunits, the surface glycoprotein subunit gp120 and the transmembrane subunit gp41.

The transmembrane Env subunits of most lentiviruses (including gp41 of HIV-1, HIV-2, and the related simian immunodeficiency viruses [SIVs]) have unusually long cytoplasmic tails (CTs) relative to those of other retroviruses, typically ~150 amino acids in length (for reviews, see references 1–3). These long CTs contain a variety of conserved motifs, including a tyrosine-based, membrane-proximal YxxØ motif (where x is any residue and Ø is a hydrophobic residue), a dileucine motif at the C terminus of the gp41 CT, and several aromatic motifs. Upon reaching the plasma membrane, Env is rapidly internalized via a clathrin-dependent pathway, mediated in part by direct interactions between the YxxØ and di-Leu motifs, and the clathrin adaptor protein complexes AP-1 and AP-2 (4–12). Rapid Env internalization limits the amount of Env displayed on the cell surface, likely reducing the detection and elimination of infected cells by the host immune response (13). Env endocytosis also contributes to the low levels of Env trimers on HIV-1 particles compared to other retroviruses, with only approximately one dozen trimers per virion (14, 15). Although some of the internalized Env may be recycled back to the cell surface after endocytic uptake (16, 17), the role of Env recycling in Env incorporation is currently unclear.

The gp41 CT has also been reported to direct the sorting of Env in polarized epithelial cells and lymphocytes (18–21), and promotes Env accumulation at points of cell-cell contact referred to as the virological synapse (VS) (22). Transfer of virus across the VS is a highly efficient route of virus transmission, at least in cell culture, relative to cell-free particle infection (23–26). As a result of this highly efficient transmission, cell-cell transfer renders HIV-1 less sensitive to replication blocks and inhibitors (27–30), and mutations that enhance cell-cell transfer reduce the susceptibility of HIV-1 to anti-retroviral drugs (31, 32).

Significantly, mutation of the YxxØ motif in the SIV_{mac239} gp41 CT allowed infected animals to control the viral infection, thereby reducing viral pathogenesis (33). Propagation of this virus *in vivo* led to the emergence of highly pathogenic revertants in which new endocytosis/trafficking motifs were acquired (34). Thus, the highly conserved endocytosis/trafficking motifs in lentiviral gp41 CTs play an important role in lentivirus propagation and pathogenesis.

In addition to playing a key role in Env trafficking and cell-surface expression, the long gp41 CT also mediates Env incorporation into virus particles (for reviews, see references 1–3 and 35). Truncation of the HIV-1 gp41 CT has little effect on Env incorporation in adherent cell lines such as HeLa and 293T and in the MT-4 T-cell line, while the gp41 CT truncation mutant (36) is severely impaired for Env incorporation, particle infectivity, and virus spread in most T-cell lines, primary T cells, and monocyte-derived macrophages (37, 38). Mutation of the aforementioned highly conserved YxxØ and di-Leu motifs in the gp41 CT has also been reported to disrupt Env incorporation, particle infectivity, and virus propagation (33, 39, 40).

The MA domain of Gag plays a central role in HIV-1 Env incorporation (36, 37, 41–44; for reviews, see references 1, 3, and 45) and is thought to organize into hexamers of trimers on the inner leaflet of the viral envelope (46–48). Recent cryo-electron tomography data suggest that MA reorganizes during virus maturation, perhaps modulating Env function during the infection process (49). Recent structural studies have also provided

insights into the conformation of the gp41 CT with respect to the membrane (50, 51), although how the gp41 CT might engage with the underlying MA lattice remains incompletely understood. It has been reported that the Gag lattice traps Env at the site of virus assembly and that a MA mutation that blocks Env incorporation (36) prevents Env trapping in the assembling Gag lattice (52).

Rab proteins are members of the Ras superfamily of small GTPases (for reviews, see references 53 and 54). They function in a cascade-like fashion in the endolysosomal and secretory pathways to regulate membrane trafficking by promoting vesicle formation, movement, and fusion. Approximately 70 Rab proteins are expressed in human cells. Rab functions are mediated via the interaction of activated (GTP-bound) Rab proteins with a number of effectors that include tethering complexes, molecular motors, scaffolding proteins, and lipid kinases and phosphatases (55–57).

The cell type-dependent role of the long gp41 CT in Env incorporation and virus replication supports the hypothesis that the CT interacts with host cell factors that regulate Env trafficking, surface expression, and virion incorporation. One such proposed gp41 CT-interacting host factor is Rab11-family interacting protein 1C (FIP1C; also known as Rab-coupling protein [RCP]). The FIPs are a family of effector proteins for Rab and ADP ribosylation factor (Arf) GTPases (for reviews, see references 58 and 59). Depletion of FIP1C by using a small hairpin RNA (shRNA) was shown to reduce Env incorporation into HIV-1 particles in HeLa cells, in the H9 T-cell line, and in primary monocyte-derived macrophages (60, 61). In contrast, FIP1C did not affect the incorporation of the gp41 CT-truncated mutant CTdel144 (60–62). FIP1C depletion also delayed HIV-1 replication in H9 cells (60, 61). Depletion of Rab14, but not Rab11, also reduced Env incorporation in HeLa cells (60). Although a direct interaction between HIV-1 Env and FIP1C was not demonstrated, expression of full-length, but not CT-truncated, Env in HeLa cells induced a redistribution of FIP1C from a perinuclear compartment to the plasma membrane (60). The ability of HIV-1 Env to relocate FIP1C was shown in a subsequent study to be dependent upon a Tyr-based motif, Y₇₉₅W, in the gp41 CT, implicating this motif in FIP1C-dependent Env incorporation (61). Furthermore, overexpression of a dominant negative fragment of FIP1C trapped wild-type (WT), but not CT-truncated or Y₇₉₅W/SL-mutant Env, in a perinuclear recycling compartment in HeLa cells (62). Together, these results supported the hypothesis that FIP1C-mediated recycling of Env is required for Env incorporation and implicated the Y₇₉₅W motif in FIP1C-mediated Env recycling to virus assembly sites on the plasma membrane.

To evaluate the role of FIP1C in HIV-1 replication in T-cell lines and primary CD4⁺ T cells, we used CRISPR-Cas9 technology to knock out the *FIP1C* gene. The results indicated variable and cell-type-dependent effects of *FIP1C* knockout (KO) on HIV-1 replication in T-cell lines and no defect in virus replication in primary CD4⁺ T cells. Mutation of the Y₇₉₅W motif in the gp41 CT impaired Env incorporation irrespective of whether FIP1C was expressed. Overall, while the results support some role for FIP1C in Env incorporation, they indicate that other, or additional, host cell factors are likely involved. The results also indicate that the Y₇₉₅W motif plays a role in Env incorporation and virus propagation that is independent of FIP1C.

RESULTS

Knockdown of FIP1C expression in HeLa cells modestly reduces virion incorporation of WT Env but not incorporation of CTdel144 or Y₇₉₅W/SL Env mutants. HIV-1 replication in most T-cell lines is abrogated by truncation of the gp41 CT (37, 38, 63, 64). Several studies have shown that mutating a hydrophobic motif, Tyr₇₉₅Trp (Y₇₉₅W), located in the LLP3 domain of the gp41 CT, to Ser-Leu (Y₇₉₅W/SL) (Fig. 1A) significantly reduces Env incorporation (39, 61, 62). This motif has been implicated in FIP1C-mediated trafficking of Env to viral assembly sites (60–62).

To begin our investigation into the role of FIP1C in the incorporation of WT and mutant Env, HeLa cells were treated with small interfering RNA (siRNA) targeting FIP1C (siFIP1C) or a nontargeting control (NT) (Fig. 1B) and were transfected with the pNL4-3 molecular clone encoding WT, CT-truncated (CTdel144) (36), or Y₇₉₅W/SL Env (Fig. 1C).

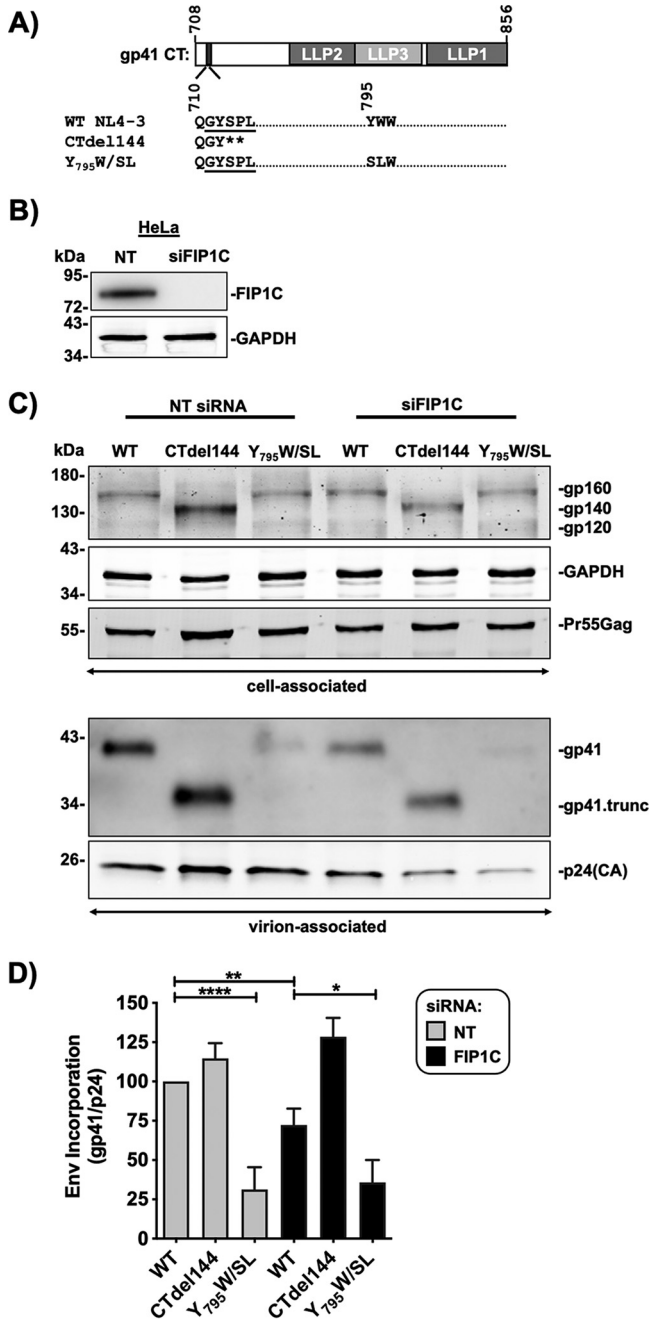


FIG 1 Knockdown of FIP1C expression in HeLa cells modestly reduces virion incorporation of WT Env but not incorporation of CTdel144 or Y₇₉₅W/SL Env mutants. (A) Schematic representation of the NL4-3 gp41 CT and gp41 CT genotypes used in this study. The lentiviral lytic peptide (LLP) domains are indicated in gray boxes, and the highly conserved tyrosine endocytosis motif is indicated with a black rectangle. The numbers above the gp41 CT schematic indicate the first and last amino acid positions of the gp41 CT. The numbers below the gp41 CT indicate the positions of the QGYSPL sequence and the Y₇₉₅W motif. The CTdel144 mutant was generated by introducing two stop codons in the highly conserved tyrosine endocytosis motif, GYSPL, resulting in a CT of 4 amino acids (36). (B) Cell lysates of HeLa cells treated with either NT or FIP1C-targeting siRNA were analyzed by Western blotting for FIP1C expression. (C) HeLa cells treated with siRNA were transfected with either WT or CTdel144 proviral DNA, and samples were collected 48 h posttransfection. Western blotting was performed on the virus fraction to detect gp41 and p24(CA) using equal amounts of WT and CTdel144 viral lysates. CTdel144 was indicated by the shift in the molecular weight of Env and labeled as gp41.trunc and gp140. (D) Env incorporation, calculated by determining the ratio of virion-associated gp41 to p24 (CA) relative to the WT condition, is represented. The values are means and standard deviations from three independent experiments. Statistical significance was assessed by one-way ANOVA and Tukey's multiple-comparison test. *, $P < 0.05$; **, $P < 0.01$; ****, $P < 0.0001$.

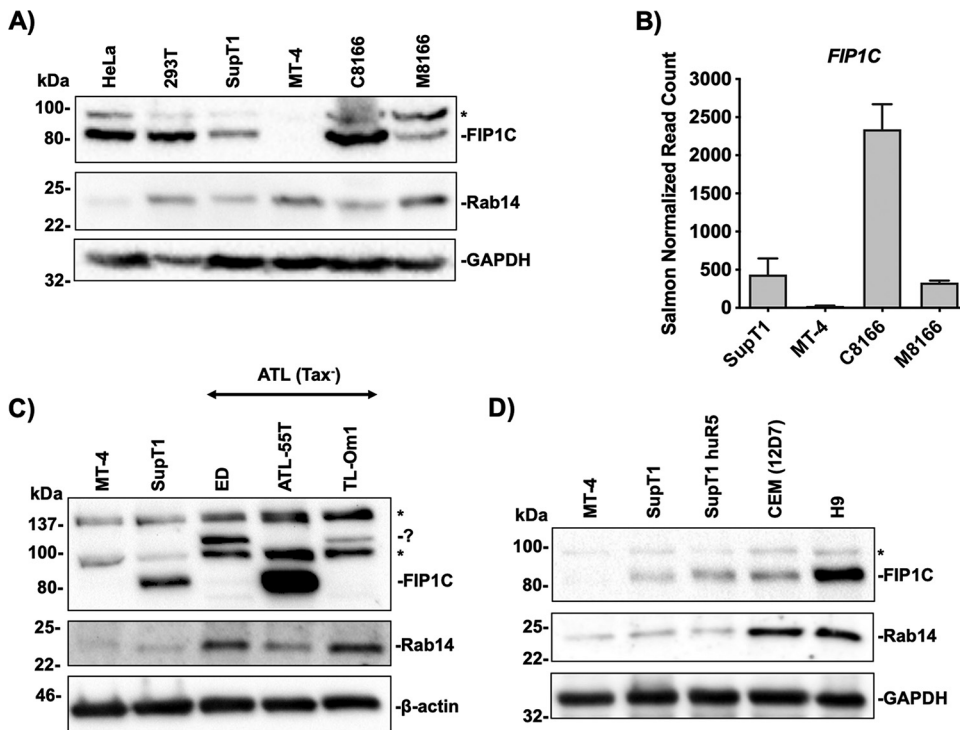


FIG 2 FIP1C is expressed in non-HTLV transformed T-cell lines. (A, C, and D) Equivalent numbers of cells were used to generate the cell lysates and equivalent volumes of lysate were analyzed by Western blotting for FIP1C, Rab14, and a loading control, either GAPDH or β -actin. Proteins were detected via chemiluminescence. (B) RNA levels were determined by Illumina RNA-seq, and RPKM values for each cell line were graphed. Western blot analysis is representative of three independent experiments. RNA-seq values are representative of duplicate RNA-seq analysis. Background bands are indicated by asterisks, and potential FIP isoforms, or background bands, are indicated with a question mark.

The siRNA-mediated knockdown was highly efficient, as no FIP1C was detectable in siFIP1C-treated cells (Fig. 1B). Cell and virus fractions were analyzed by Western blotting to detect virally encoded proteins (Fig. 1C). FIP1C knockdown (KD) did not affect levels of cell-associated Env expression but resulted in an approximately 25% reduction in WT Env incorporation without any reduction in the incorporation of CTdel144 or Y₇₉₅W/SL Env (Fig. 1D). While the effects of FIP1C KD on WT Env incorporation were modest, this result is consistent with the previously described role for FIP1C in HIV-1 Env incorporation in HeLa cells (60–62).

FIP1C is expressed in non-HTLV-transformed T-cell lines. FIP1C expression in human T-cell lines has been reported in H9 (60) and CEM-SS T-cell lines (65). To measure FIP1C protein expression in cell lines commonly used in the study of HIV-1 replication, we performed Western blotting using a range of cell lines (Fig. 2A). We also examined the expression levels of Rab14, which has been implicated in Env incorporation (60). HeLa cells were used as a positive control for FIP1C expression. FIP1C expression in HeLa and 293T was approximately equivalent, while FIP1C protein levels in the T-cell lines tested—SupT1, C8166, and M8166—varied. Consistent with a previous report (65), and despite being highly permissive for HIV-1 replication (64, 66), MT-4 cells did not express detectable levels of FIP1C. All four T-cell lines expressed Rab14. To further interrogate the defect in FIP1C gene expression in MT-4 cells, transcriptome sequencing (RNA-seq) was performed to measure RNA levels of the FIP1C isoform (Fig. 2B). RNA levels closely mirrored protein levels (Fig. 2A and B), indicating that the defect in FIP1C protein expression in MT-4 cells is due to a lack of FIP1C RNA expression.

MT-4 is a human T-cell leukemia virus type 1 (HTLV-1)-transformed cell line (67) that expresses HTLV-1 Tax (64, 66, 68). To examine whether FIP1C and Rab14 expression may be influenced by HTLV-1 transformation and determine their expression levels

across previously unevaluated T-cell lines permissive to HIV-1 replication, FIP1C and Rab14 expression in other HTLV-1-transformed T-cell lines was evaluated (Fig. 2C). Western blotting was performed to measure FIP1C and Rab14 expression in several adult T-cell leukemia/lymphoma (ATL) cells that express little or no detectable Tax protein (Tax⁻) (64), though some of these cell lines (e.g., TL-Om1 and ED) were permissive to HIV-1 replication (69). The FIP1C-deficient MT-4 and FIP1C-expressing SupT1 cells were included as negative and positive controls, respectively. Two of the ATL Tax⁻ cell lines, ED and TL-Om1, did not express FIP1C but instead expressed an additional band with a higher molecular weight, approximately 95 kDa. This additional band, which could be a background band or an additional FIP isoform, was not present in the MT-4 or SupT1 samples. ATL-55T cells expressed high levels of FIP1C and did not express this additional band of higher molecular weight. FIP1C expression was not linked to Rab14 protein expression, as all tested ATL Tax⁻ cell lines expressed Rab14, albeit at various levels (Fig. 2C).

To assess FIP1C and Rab14 expression across non-ATL T-cell lines, Western blotting was performed on SupT1huR5, CEM(12D7), and H9 cell lysates (Fig. 2D). FIP1C and Rab14 expression levels varied among these cell lines, with FIP1C and Rab14 expression being highest in H9. Altogether, these data indicate that FIP1C is expressed in all non-HTLV-1 transformed human T-cell lines tested, while FIP1C expression is deficient in 3 of the 6 HTLV-1-transformed cell lines tested. Additionally, Rab14 was expressed in all T-cell lines tested. Importantly, despite being highly permissive for HIV-1 replication, the MT-4 T-cell line does not express detectable levels of FIP1C. Altogether, these data show that FIP1C is not required for T-cell permissivity to HIV-1 replication.

FIP1C KO in Jurkat E6.1 cells does not impair Env incorporation or viral replication kinetics. A role for FIP1C in HIV-1 replication in the H9 T-cell line was demonstrated by using shRNA-mediated knockdown of FIP1C expression (60). To determine whether FIP1C is required for Env incorporation in the Jurkat E6.1 T-cell line, CRISPR-Cas9 gene editing was used to generate two single-cell-derived FIP1C knockout (KO) clones, denoted KO clones 6 and 9 (Fig. 3A). No FIP1C protein expression was detected in either KO clone by Western blotting (Fig. 3B). Env incorporation in the FIP1C KO cell lines was compared to that in the parental cell line (Fig. 3B). FIP1C KO did not alter Env incorporation in KO clone 6, but KO clone 9 incorporated 200% more WT Env than parental cells or KO clone 6 (Fig. 3B and C). Clone 9 also displayed an overall increase in viral protein expression (Gag and Env). The Y₇₉₅W/SL mutant displayed reduced Env incorporation relative to WT, consistent with a role for this motif in Env incorporation (39, 61, 62). However, as in the case of WT Env, FIP1C KO did not reduce incorporation of this Env mutant (Fig. 3B).

To determine whether FIP1C KO affects viral infectivity independently of virion Env content, cell-free infectivity of released virus was determined (Fig. 3D). Virus particles produced from Jurkat E6.1 KO clone 6 displayed WT levels of infectivity, whereas, consistent with increased Env content, viruses produced from KO clone 9 were 250% more infectious than WT virions produced from parental cells. The infectivity of Y₇₉₅W/SL mutant virions produced from the KO clones either was not different from the infectivity of this mutant produced in parental cells (clone 6) or displayed increased infectivity (clone 9, consistent with the increase in Env incorporation in this clone). Thus, while the Y₇₉₅W/SL mutant displayed reduced infectivity relative to WT in the Jurkat E6.1 cell line, this reduced infectivity was not linked to FIP1C expression.

To compare the replication of WT HIV-1 in the parental and KO Jurkat E6.1 clones, cells were transfected with WT pNL4-3 and replication kinetics were monitored by a reverse transcriptase (RT) assay (Fig. 3E). WT HIV-1 replication in KO clone 6 peaked 3 days earlier than in parental Jurkat E6.1 cells. In KO clone 9, virus replicated with substantially faster kinetics than in parental cells, consistent with increased viral gene expression, higher Env content, and increased infectivity of virus produced in this cell clone. Altogether, these findings demonstrate that FIP1C is not required for Env incorporation or HIV-1 replication in the Jurkat E6.1 T-cell line. The increases in viral gene

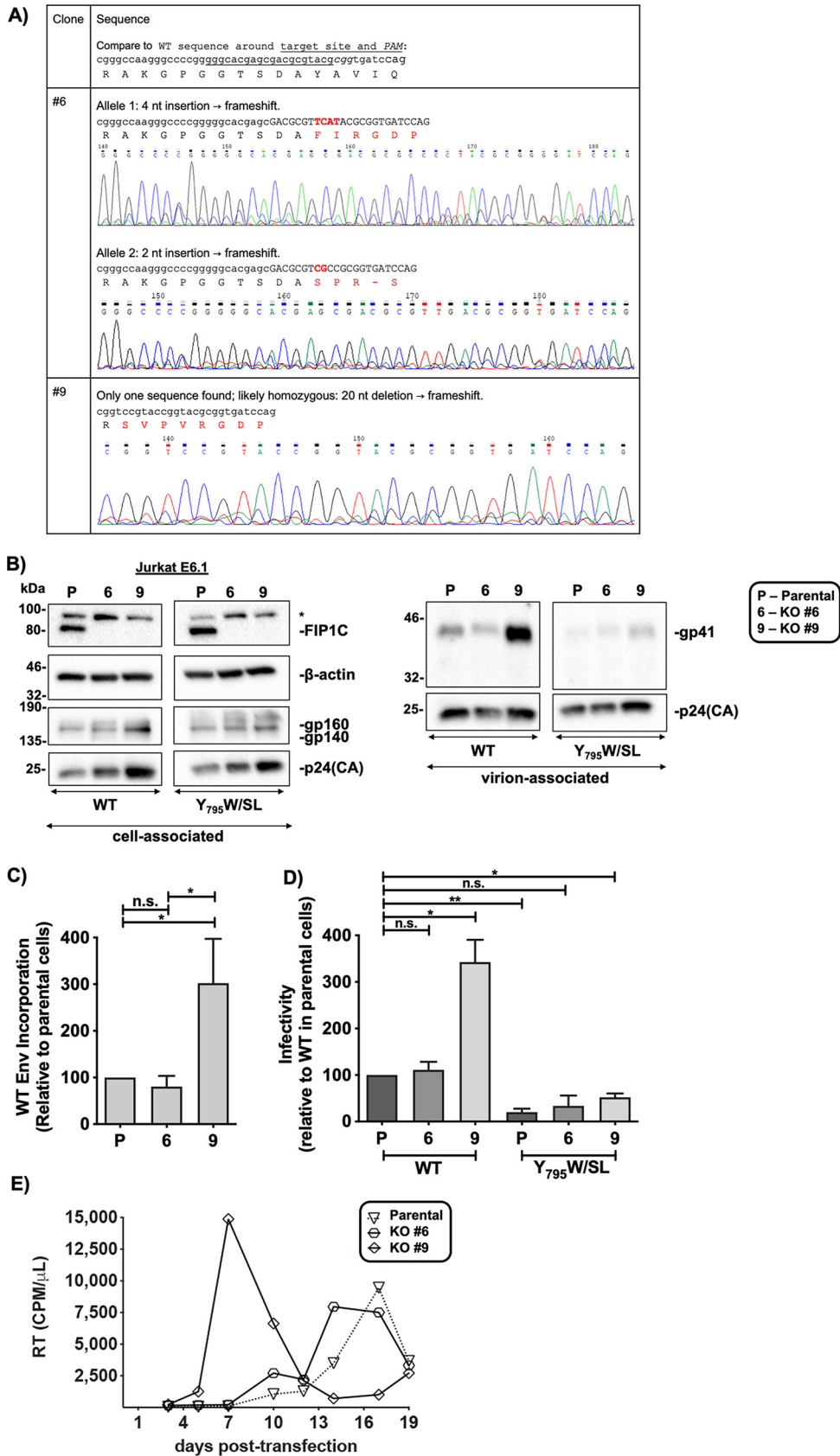


FIG 3 FIP1C KO in Jurkat E6.1 cells does not impair Env incorporation or viral replication kinetics. (A) Bold red in the nucleotide sequences represents inserted nucleotides. In the protein sequences, red represents (Continued on next page)

expression relative to parental cells in KO clone 9 also highlight the potential pitfalls associated with single-cell-derived clones (see Discussion).

FIP1C KO in the SupT1 T-cell line modestly reduces viral protein expression and Env incorporation but does not affect virus replication kinetics. The data presented in Fig. 3 indicate that FIP1C is not required for HIV-1 Env incorporation or virus replication in the Jurkat E6.1 T-cell line. To examine the role of FIP1C in another T-cell line, we generated FIP1C KOs in the CCR5-expressing SupT1 T-cell line SupT1huR5. To avoid the clonal variability observed with the single-cell-derived Jurkat E6.1 KO clones (see above), we generated a polyclonal FIP1C KO SupT1huR5 cell lines. A cell line expressing Cas9, but not the guide RNA (gRNA), was also generated for use as a control (CTRL). FIP1C expression was undetectable by Western blotting in the FIP1C KO SupT1huR5 cell line but readily detectable in the Cas9-expressing CTRL line (Fig. 4A).

To determine the effect of FIP1C KO on Env incorporation, CTRL and FIP1C KO SupT1huR5 cells were transduced with vesicular stomatitis virus protein G (VSV-G)-pseudotyped NL4-3 encoding either WT or Y₇₉₅W/SL Env. Cell and viral lysates were analyzed for Gag and Env expression by Western blotting (Fig. 4A). The cellular Env/Gag ratio (Fig. 4B) and the cellular Gag expression relative to glyceraldehyde-3-phosphate dehydrogenase (GAPDH) of WT virus in FIP1C KO cells relative to CTRL cells were determined by Western blotting (Fig. 4C). The results indicated that the ratio of Env to Gag and Gag expression overall were lower in FIP1C KO cells than CTRL cells. Reductions in Env incorporation [the ratio of gp41_v to p24(CA)_v, where “v” denotes virion-associated protein] were likewise observed with reduced Env incorporation partially due to reduced Env expression in the FIP1C KO cells. There was an approximately 41% reduction in WT Env incorporation efficiency, defined as $[\text{gp41}_{\text{v}}/\text{p24(CA)}_{\text{v}}]/(\text{gp120}_{\text{c}} + \text{gp160}_{\text{c}})$, where “c” and “v” denote cell- and virion-associated protein, respectively (Fig. 4D).

We also compared the Env incorporation efficiency for the Y₇₉₅W/SL mutant in SupT1 FIP1C KO versus CTRL cells. The Y₇₉₅W/SL mutant exhibited a significant, and comparable, reduction in Env incorporation in both FIP1C KO and CTRL cells (Fig. 4E). Cell-free, single-cycle infectivity of the virions generated in these cells was also calculated. TZM-bl cells were infected with RT-normalized virus, and luciferase expression was quantified and normalized to CTRL-WT conditions (Fig. 4F) and relative to WT conditions for each cell line (Fig. 4G). The cell-free infectivity data paralleled the virion Env incorporation levels (compare Fig. 4F and E). When values were normalized to WT conditions for each cell line, the defect imposed by the Y₇₉₅W/SL mutant was essentially identical in CTRL and FIP1C KO cell lines (Fig. 4G). Altogether, these data indicate that mutation of the Y₇₉₅W motif caused a significant reduction in Env incorporation that is independent of FIP1C expression and that FIP1C KO caused modest effects on Env expression that contributed to the observed reductions in Env incorporation.

We next examined the effect of FIP1C KO on NL4-3 replication kinetics in SupT1 cells. The CTRL and FIP1C KO cells were transfected with WT, a mutant not expressing Env (Env⁻), or Env Y₇₉₅W/SL NL4-3 proviral clones, and virus replication was monitored by RT assay (Fig. 5A). As expected, the Env⁻ NL4-3 derivative did not replicate in either CTRL or KO cells. The NL4-3 WT clone replicated in CTRL and FIP1C KO cells with essentially identical kinetics, indicating

FIG 3 Legend (Continued)

frameshifted residues. (B) Cells were transduced with RT-normalized VSV-G-pseudotyped NL4-3 encoding either WT or Y₇₉₅W/SL Env. Western blotting was performed on the cell fraction to detect FIP1C, the Gag precursor Pr55Gag, p24(CA), and gp160 and on the virus fraction to detect gp41 and p24(CA) using equal amounts of viral lysates. (C) Relative Env incorporation was calculated by determining the ratio of virion-associated gp41 to p24(CA) relative to WT. (D) RT-normalized Viral supernatants were used to infect TZM-bl cells. Luciferase values were then used to determine the relative infectivity of virus produced from each Jurkat E6.1 T-cell line. Values are means and standard deviations for virions produced from KO cell lines for WT and Y₇₉₅W/SL Env genotypes. (E) Replication curves for spreading infection of WT NL4-3 in parental and KO Jurkat E6.1 cell lines were compared. Cell lines were transfected with the proviral clone, split 1/3, and replenished with fresh RPMI-10% FBS every 2 to 3 days. An aliquot of the cell culture supernatant was reserved for analysis of HIV-1 RT activity at each time point. Replication kinetics are representative of 3 independent experiments. Statistical significance was assessed by Student's *t* test. *, *P* < 0.05; **, *P* < 0.01; n.s., no statistical significance.

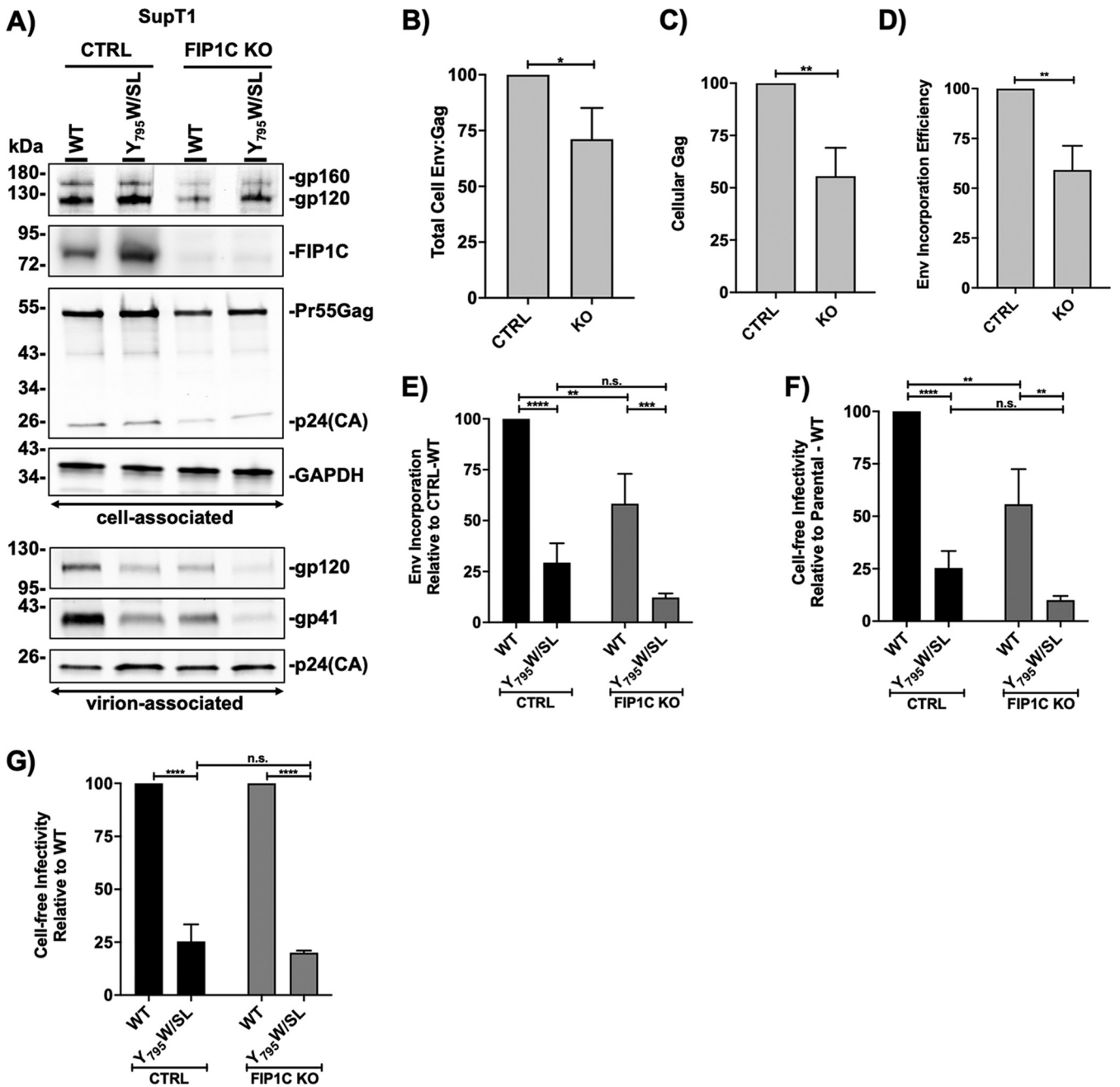


FIG 4 FIP1C KO in the SupT1 T-cell line modestly reduces viral protein expression and Env incorporation. (A) Cells were transduced with RT-normalized VSV-G-pseudotyped NL4-3 encoding either WT or YW₇₉₅SL Env. Western blot analysis was performed on the cell fraction to detect FIP1C and viral products and on the virus fraction to detect viral products using equal amounts of viral lysates. Various endpoints were measured from the band intensities on the Western blots. (B) The cellular Env/Gag ratio was calculated as $(gp120_c + gp160_c) / [Pr55(Gag)_c + p24(CA)_c]$. (C) Cellular Gag expression was calculated as $[Pr55(Gag)_c + p24(CA)_c] / GAPDH_c$. (D) Env incorporation efficiency was calculated as $[gp41_v / p24(CA)_v] / [gp120_c + gp160_c]$. (E) Env incorporation was calculated as $gp41_v / p24(CA)_v$. In all formulas, “c” is cell and “v” is virus. (F and G) Viral supernatants were RT normalized, and a serial dilution of virus was used to infect TZM-bl cells. Luciferase values were then used to determine the relative infectivity of virus produced from each T-cell line. The bar graphs show the mean infectivity values of virions produced from the control (CTRL) and the KO cell lines for WT and YW₇₉₅SL Env genotypes from both cell lines relative to (F) WT virions produced by CTRL cells or (G) WT produced by either cell line. The control cell lines express Cas9 but are otherwise unmodified. Data are representative of three independent experiments. Statistical significance was assessed by Student’s *t* test. *, *P* < 0.05; **, *P* < 0.01; ***, *P* < 0.001; ****, *P* < 0.0001; n.s., no statistical significance.

that FIP1C is not required for the spread of NL4-3 in SupT1 huR5 cultures. The Y₇₉₅W/SL mutant replicated with similarly delayed kinetics in CTRL and KO cells, indicating that the replication defect exhibited by the Y₇₉₅W/SL mutant in this T-cell line is unrelated to FIP1C expression.

The Y₇₉₅W motif is highly conserved among subtype B viruses, whereas only Y₇₉₅ is

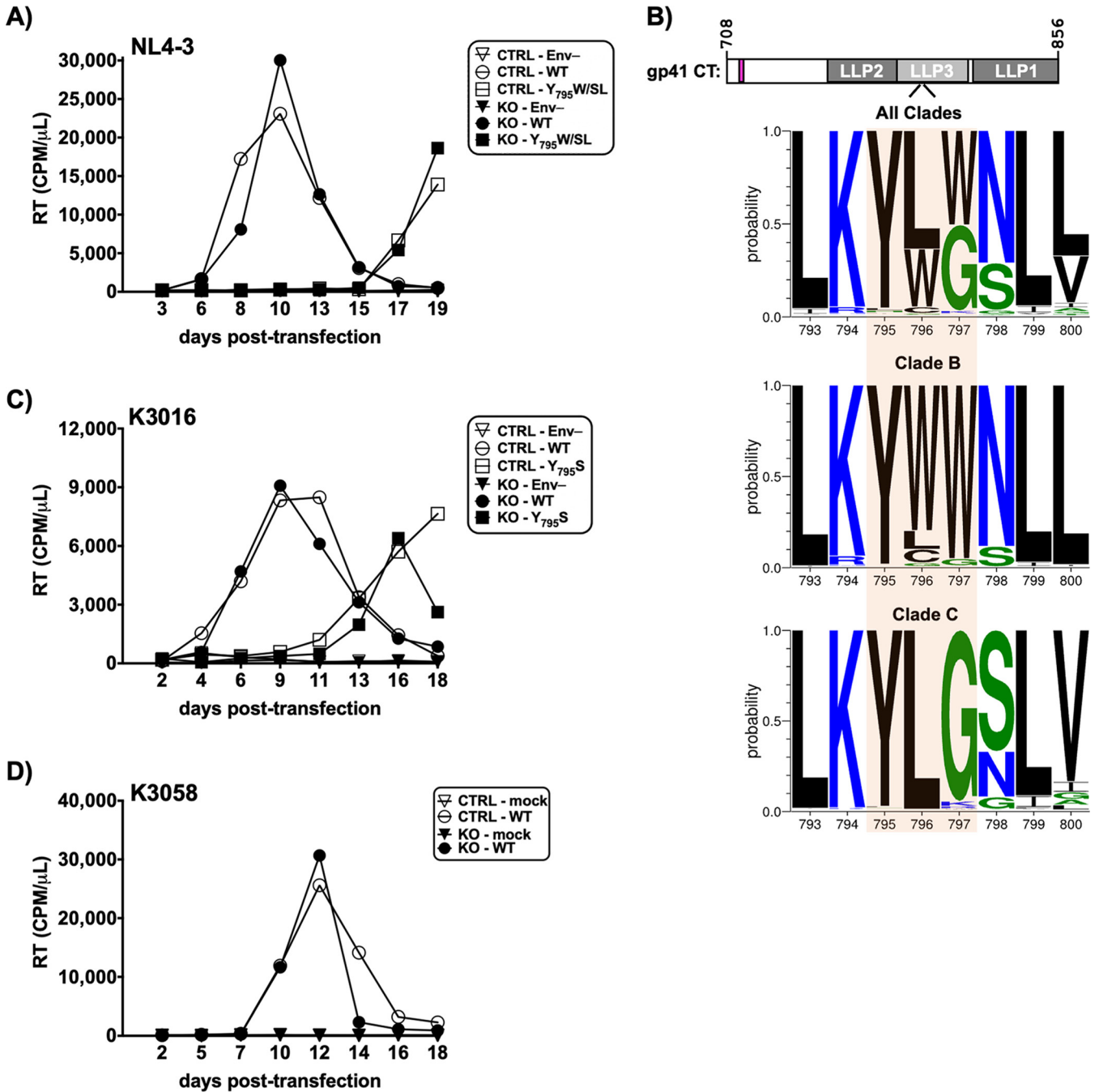


FIG 5 FIP1C KO in SupT1 does not affect viral replication kinetics of NL4-3 and clade C transmitted/founder HIV-1 strains K3016 and K3058. (A, C, and D) Replication curves for spreading infection of WT and Y₇₉₅W/SL NL4-3, WT and Y₇₉₅S K3016, and WT K3058. NL4-3 replications were performed in SupT1 cells, and K3016 and K3058 replications were performed in SupT1huR5 cells. Cell lines were transfected with the proviral clone, split 1/3, and replenished with fresh RPMI-10% FBS every 2 to 3 days. An aliquot of the cell culture supernatant was reserved for analysis of HIV-1 RT activity at each time point. Data are representative of three independent experiments. (B) Schematic representation of the NL4-3 gp41 CT and gp41 CT genotypes used in this study. The lentiviral lytic peptide (LLP) domains are indicated in gray boxes, and the highly conserved tyrosine endocytosis motif is indicated with a shaded pink rectangle. The numbers above the gp41 CT schematic indicate the first and last amino acid positions of the gp41 CT. The frequencies of amino acids by position of HIV-1 sequences in the Los Alamos database are shown for all clades, clade B, or clade C. The conserved aromatic patch in LLP3 is indicated by the orange region overlapping with amino acids 795-797.

conserved in subtype C viruses, with residue 796 frequently being a Leu rather than a Trp (Fig. 5B). Among the >6,000 subtype B Env amino acid sequences in the Los Alamos National Laboratory (LANL) database at the time of this analysis (70), Y₇₉₅ is 98.24% conserved, and among sequences across all subtypes, Y₇₉₅ is 96.74% conserved.

Due to the high degree of conservation of Y₇₉₅ and absence of W at position 796 in subtype C viruses, a Y₇₉₅S mutant was generated in the subtype C transmitted/founder strain K3016. CTRL and FIP1C KO SupT1huR5 cells were transfected with K3016 proviral clones expressing either WT Env or the Y₇₉₅S mutant, and virus replication was monitored (Fig. 5C). The WT K3016 clone replicated with identical kinetics in CTRL and FIP1C KO cultures, indicating that FIP1C is not required for the spread of K3016 in SupT1huR5 cultures. The Y₇₉₅S mutant exhibited similarly delayed replication in both the CTRL and FIP1C KO cells, indicating that the replication defect imposed by the Y₇₉₅S mutation in the context of the K3016 isolate is unrelated to FIP1C expression. The effect of FIP1C KO on the replication of another subtype C transmitted/founder virus, K3058, was also evaluated (Fig. 5D). FIP1C KO did not alter virus replication kinetics for this isolate. Altogether, these data indicate that FIP1C expression is not required for the spread of NL4-3, K3016, or K3058 strains in the SupT1huR5 T-cell line. Furthermore, mutation of the Y₇₉₅W motif in NL4-3 and Y₇₉₅ in K3016 resulted in replication defects that were unaffected by FIP1C KO, similar to NL4-3 and the NL4-3 Y₇₉₅W/SL Env mutant.

FIP1C KO in H9 cells results in reduced viral protein expression and Env incorporation and attenuated virus replication. As mentioned above, shRNA-mediated knockdown of FIP1C in H9 cells was demonstrated to delay HIV-1 replication (60). To corroborate these results by using CRISPR-Cas9 KO technology, a polyclonal FIP1C KO H9 cell line was generated by using the same method employed for SupT1huR5. In this case, we used the parental cells as a control. FIP1C was detected by both fluorescence- and chemiluminescence-based Western blotting, the latter being the more sensitive detection method. FIP1C was not detected by either method (Fig. 6A), indicating a highly efficient KO. Due to the utilization of different blocking buffers in these two detection methods, the pattern of background bands was different (Fig. 6A, asterisks).

We next assessed the effect of FIP1C KO on Env incorporation in H9 cells. Parental and FIP1C KO H9 cells were transduced with VSV-G-pseudotyped NL4-3 encoding WT Env. Cell and viral fractions were analyzed by Western blotting (Fig. 6B). From these blots, the cellular Env/Gag ratio (Fig. 6C) and cellular Gag expression relative to GAPDH (Fig. 6D) in FIP1C KO H9 cells relative to parental cells were determined. We found that the Env/Gag ratio, Env expression, and Gag expression were lower in FIP1C KO cells than parental cells, similar to the phenotype observed in SupT1huR5 KO cells. The effect on Env expression was greater than the effect on Gag expression. To quantify Env incorporation in the FIP1C KO cells, the percent Env incorporation relative to the parental cells was calculated as was done with SupT1 cells. FIP1C KO resulted in an approximately 66% reduction in Env content in virions (Fig. 6E). To determine whether the reduced Env/Gag ratio contributed to the reduced virion Env content, we calculated the Env incorporation efficiency in FIP1C KO versus parental cells (Fig. 6F), as was done with SupT1 cells. After performing this normalization for cell-associated Env levels, we calculated a small (~30%) but statistically significant reduction in Env incorporation efficiency, which indicates that the Env incorporation defect in the H9 FIP1C KO cell line is at least partially due to reduced Env expression.

To determine the effect of FIP1C KO on HIV-1 replication in H9 cells, parental and KO cells were transfected with NL4-3 proviral clones encoding either Env⁻, WT, or Y₇₉₅W/SL Env. Virus replication was monitored by supernatant RT levels (Fig. 7A and B). In both the parental and FIP1C KO cells, Env⁻ NL4-3 did not replicate, as anticipated. The NL4-3 WT clone peaked on day 9 in the parental line but exhibited attenuated replication in the FIP1C KO cells. The Y₇₉₅W/SL mutant exhibited a dampened and delayed replication curve in the parental line and was highly defective for spreading infection in the FIP1C KO line. Therefore, in contrast to the Jurkat E6.1 and SupT1huR5 cell lines, FIP1C KO resulted in replication defects in the H9 cell line. We consistently observed less efficient replication of WT NL4-3 in H9 FIP1C KO cells than parental H9 and the other T-cell lines tested, as determined by the lower levels of RT activity at the peak of replication in H9 FIP1C KO cells.

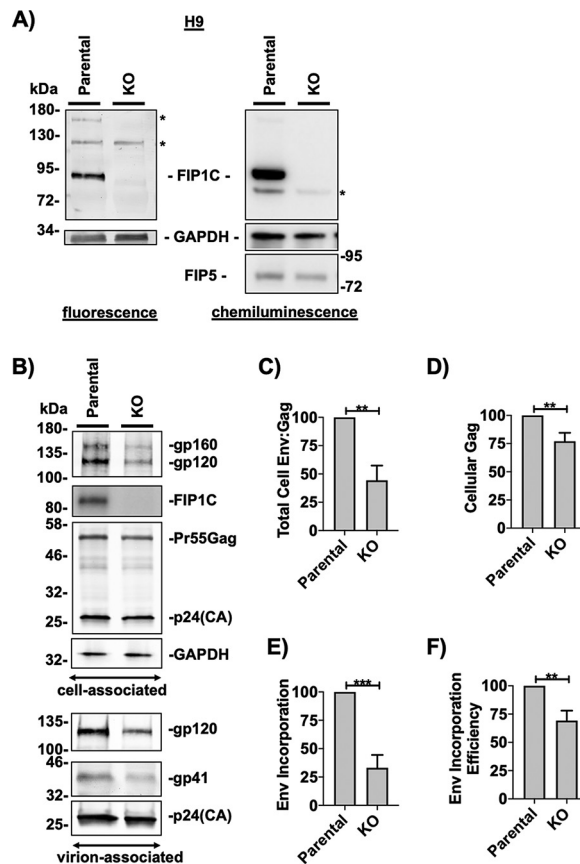


FIG 6 FIP1C KO in H9 cells results in reduced viral protein expression and Env incorporation. (A) An equivalent number of cells were lysed to generate cell lysates for analysis, and an equivalent volume of cell lysates were analyzed by Western blotting. Samples were analyzed for FIP1C expression by fluorescence and chemiluminescence (see Materials and Methods). A background band is denoted by an asterisk. (B) Cells were transfected with RT-normalized VSV-G pseudotyped NL4-3 encoding WT Env. Western blot analysis was performed on the cell fraction to detect FIP1C and viral products and on the virus fraction to detect viral products using equal amounts of viral lysates. Various endpoints were measured from the band intensities on the Western blots. (C) The cellular Env/Gag ratio was calculated as $(gp120_c + gp160_c) / [Pr55(Gag)_c + p24(CA)_c]$. (D) Cellular Gag expression was calculated as $[Pr55(Gag)_c + p24(CA)_c] / GAPDH_c$. (E) Env incorporation efficiency was calculated as $[gp41_v / p24(CA)_v] / [gp120_c + gp160_c]$. (F) Env incorporation was calculated as $gp41_v / p24(CA)_v$. In all formulas, "c" is cell and "v" is virus. Data are representative of three independent experiments. Statistical significance was assessed by Student's *t* test. **, *P* < 0.01.

Increasing cell density rescues detrimental effects of FIP1C KO on HIV-1 replication in H9 cells. A number of studies have demonstrated that, at least in cell culture, HIV-1 spreads much more efficiently via cell-cell than by cell-free transfer (see the introduction). We reasoned that increasing cell density would enhance the ability of the virus to spread via the cell-cell route. To examine this question, equal numbers of cells were transfected with equivalent amounts of NL4-3 proviral DNA encoding either WT or Y₇₉₅W/SL Env (Fig. 8) and cultured at different densities by manipulating the culture surface area. Increasing the cell density of SupT1 hu5 cultures resulted in a modest enhancement of the WT and Y₇₉₅W/SL replication peak heights of both parental and FIP1C KO cells (compare Fig. 8A and B). In contrast, increasing the cell density of H9 cultures resulted in a complete rescue of HIV spreading infection kinetics in FIP1C KO cells (compare the high-density WT curves in Fig. 8C and D). These data show that culturing cells at a high density can overcome the replication defect imposed by FIP1C KO in H9 cells.

Primary human PBMCs express FIP1C. To investigate whether FIP1C is expressed in primary human cells, and whether FIP1C expression is confined to CD4⁺ or CD4⁻ human peripheral blood mononuclear cell (hPBMC) subsets, three populations of PBMCs

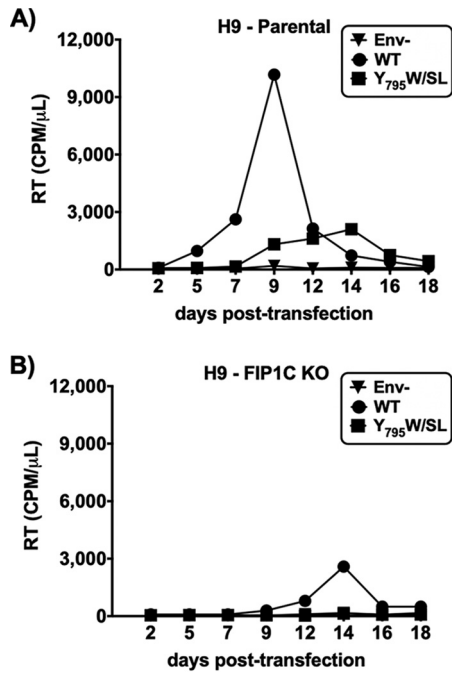


FIG 7 FIP1C KO in H9 cells results in attenuated virus replication. (A and B) Replication curves for spreading infection of WT and Y₇₉₅W/SL NL4-3 in H9 and H9 FIP1C KO cells. Cell lines were transfected with the proviral clone, split 1/3, and replenished with fresh RPMI-10% FBS every 2 to 3 days. An aliquot of the cell culture supernatant was reserved for analysis of HIV-1 RT activity at each time point. Data are representative of three independent experiments.

were generated: total, CD4⁻, and CD4⁺ cells. To generate the total hPBMC population, a fraction of the total PBMCs was separated and lysed. The remaining cells were used to generate the CD4⁺ and CD4⁻ cell populations. After CD4 enrichment and before lysing, a small portion of cells from the CD4-enriched and CD4-depleted fractions was reserved

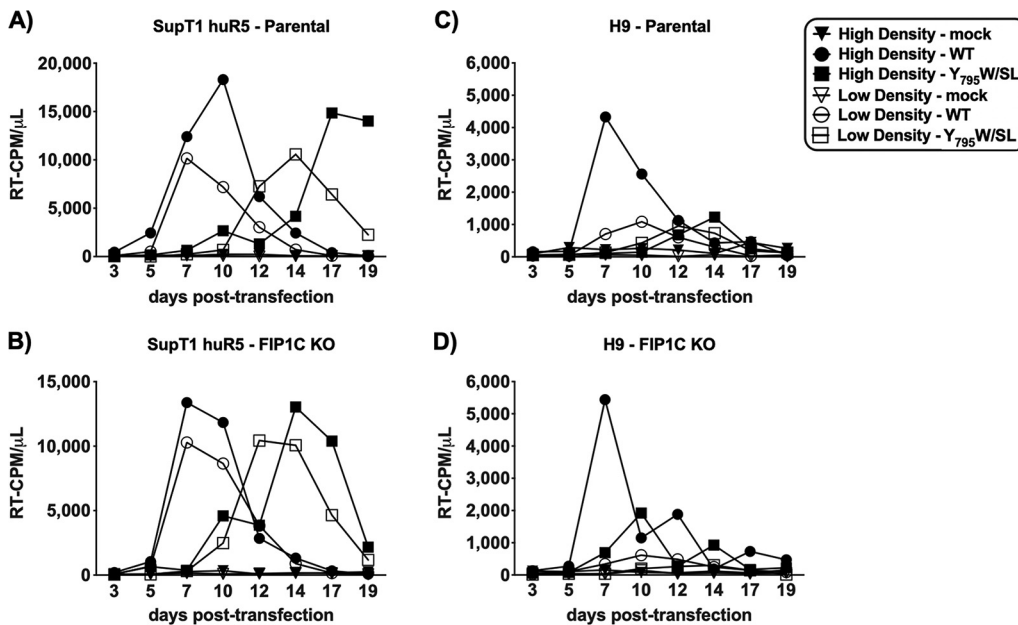


FIG 8 Increasing cell density rescues detrimental effects of FIP1C KO on HIV-1 replication in H9 cells. (A to D) Replication curves for spreading infection of WT and Y₇₉₅W/SL NL4-3 in H9 and SupT1 huR5 parental and FIP1C KO cells are shown. Cells were transfected as described in Materials and Methods. Cells were split 1/3 and replenished with fresh RPMI-10% FBS every 2 to 3 days. An aliquot of the cell culture supernatant was reserved for analysis of HIV-1 RT activity at each time point. Data are representative of three independent experiments.

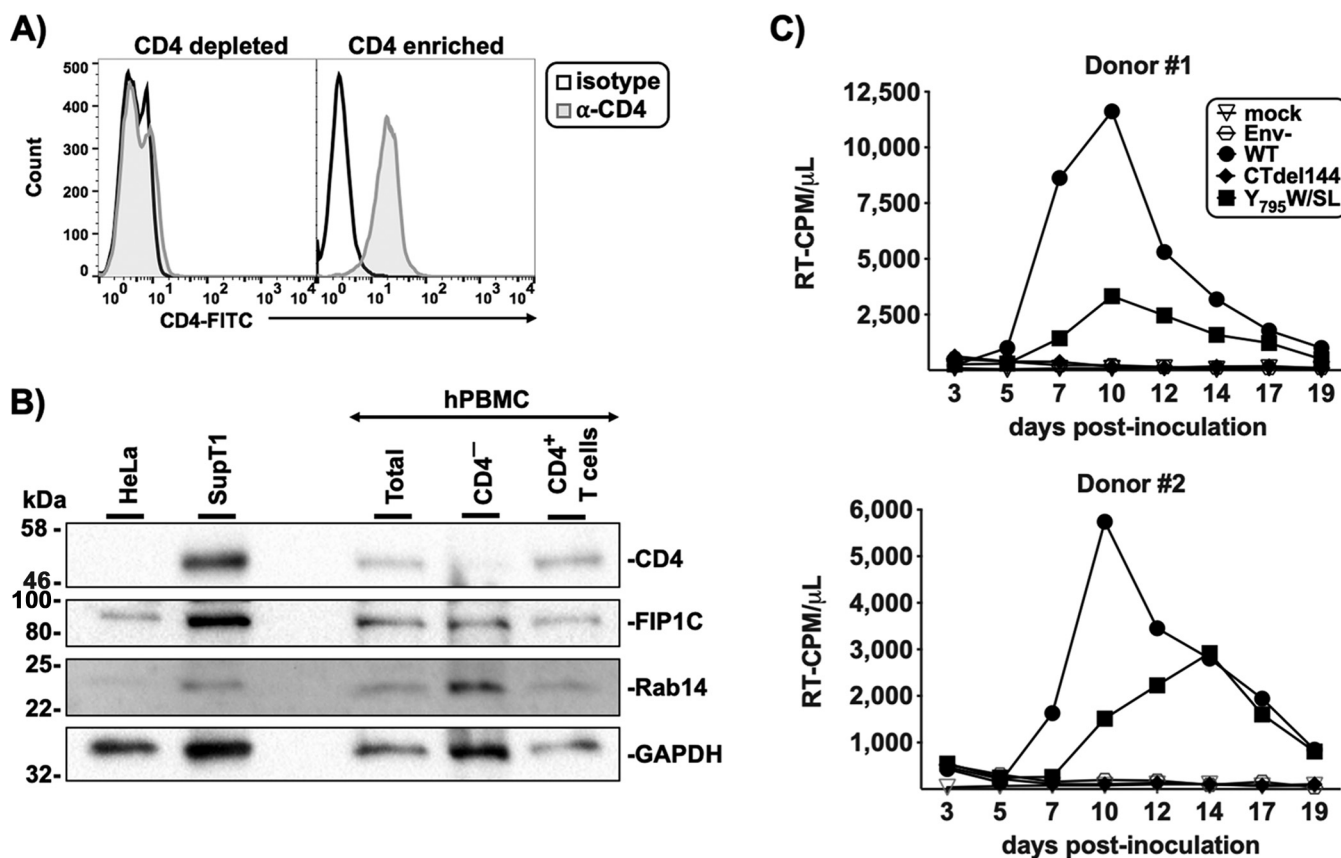


FIG 9 Primary human PBMCs express FIP1C. (A) CD4⁺ T cells were isolated from hPBMCs and analyzed by flow cytometry for CD4 expression. Data are representative of 3 donors. (B) CD4⁻ lymphocytes and CD4⁺ T cells were analyzed by Western blotting for FIP1C and Rab14 and compared to total PBMCs and FIP1C⁺ and Rab14⁺ SupT1 and HeLa cells. Data are representative of those from 3 donors. (C) hPBMCs were transduced with RT-normalized VSV-G-pseudotyped NL4-3 encoding either Env⁻, WT Env, CTdel144, or Y₇₉₅W/SL Env. Samples were acquired as described in Materials and Methods.

for cell-surface CD4 detection by flow cytometry. The results indicated that CD4 enrichment was highly efficient (Fig. 9A). The resulting three populations were analyzed for FIP1C expression by Western blotting using HeLa cells as a positive control for FIP1C expression (Fig. 9B). The SupT1 T-cell line was included to allow a comparison between primary T cells and a FIP1C expressing T-cell line. FIP1C was expressed in all PBMC populations generated, albeit at different levels. FIP1C expression in SupT1 cells was higher than in HeLa or primary cells. Rab14 was also detected in HeLa cells, SupT1 cells, and CD4⁻ and CD4⁺ PBMCs.

The results presented above and in a previous study (61) demonstrate that the Y₇₉₅W/SL mutant is replication defective in T-cell lines. To determine whether this mutant can spread in primary CD4⁺ T cells, hPBMCs were transduced with VSV-G-pseudotyped NL4-3 encoding either Env⁻, WT, CTdel144, or Y₇₉₅W/SL Env. The virus-containing supernatant was sampled every 2 to 3 days to monitor virus replication. WT virus replication peaked 10 days postinoculation, while the Env⁻ and CTdel144 Env mutants did not replicate, as expected (Fig. 9C). The Y₇₉₅W/SL Env mutant exhibited attenuated replication relative to WT, indicating that mutation of the Y₇₉₅W motif results in impaired viral spread in primary CD4⁺ T cells.

FIP1C is dispensable for NL4-3 replication in primary T cells. To determine if FIP1C is required for HIV-1 replication in primary CD4⁺ T cells, we used a CRISPR-Cas9 gene editing approach to knockout FIP1C in cells from three independent healthy blood donors. Briefly, synthetic CRISPR gRNAs were complexed *in vitro* with purified *S. pyogenes* Cas9 to form CRISPR-Cas9 ribonucleoprotein complexes, which were delivered to activated, primary CD4⁺ T cells by electroporation (Fig. 10A) (71, 72). Four gRNAs targeting FIP1C were delivered independently as well as in a multiplexed pool

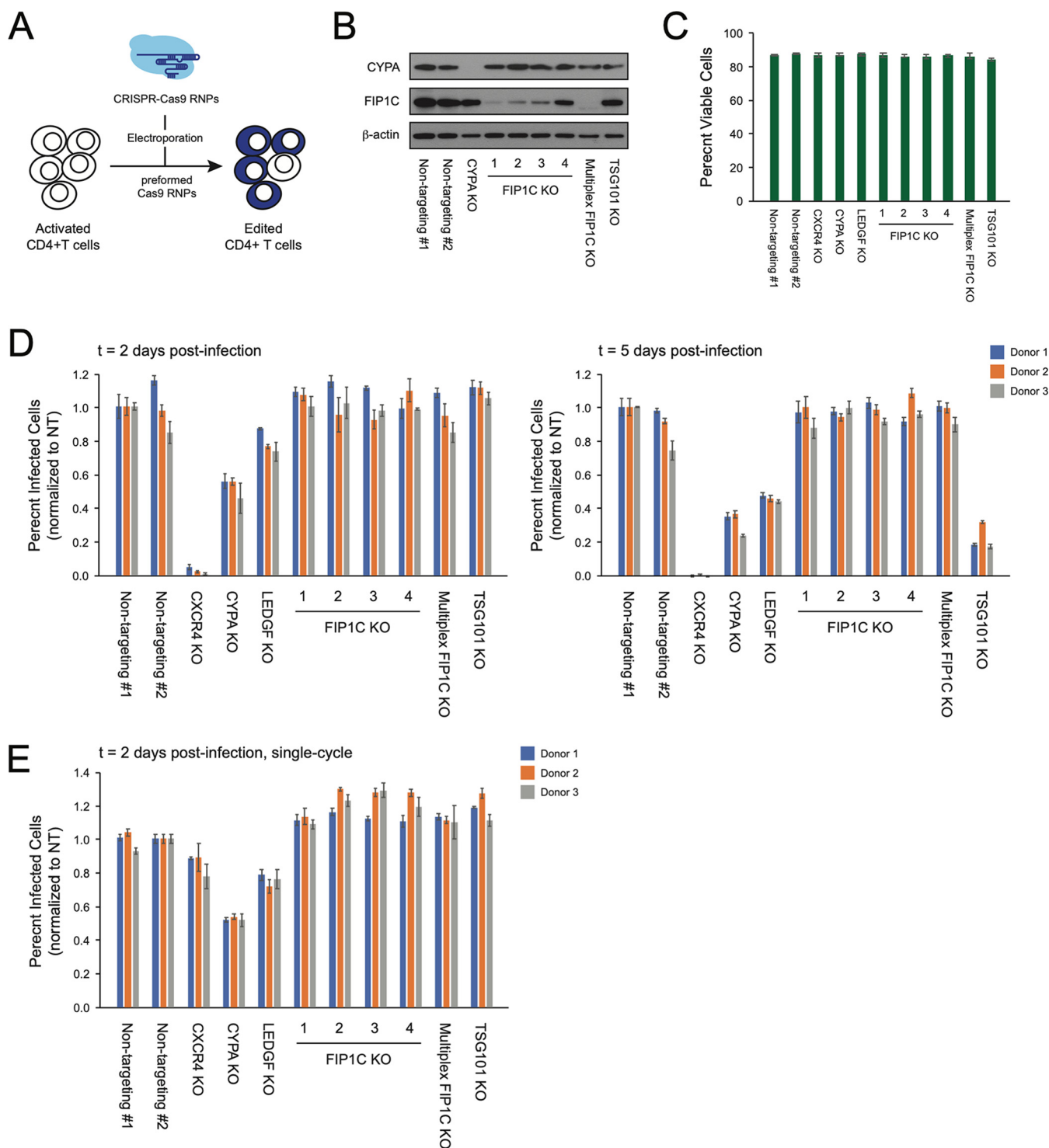


FIG 10 FIP1C is dispensable for NL4-3 replication in primary T cells. (A) Schematic of the CRISPR-Cas9 ribonucleoprotein knockout approach used for this assay. (B) Immunoblots of each indicated knockout population from one representative donor showing protein levels of CYPA and FIP1C relative to the β -actin loading control. (C) Percent viable CD4⁺ T cells in each indicated knockout population as determined by amine dye staining and flow cytometry (means and standard deviations across three donors). (D) Percent infected (GFP⁺) cells 2 (left) and 5 (right) days after challenge with HIV-1 NL4-3 nef:IRES:GFP in each indicated knockout population (means and standard deviations across three technical replicates). Data are normalized to one of two nontargeting controls. (E) Percent infected (GFP⁺) cells 2 days after challenge with VSV-G pseudotyped HIV-1 dEnv NL4-3 nef:IRES:GFP in each indicated knockout population (means and standard deviations across three technical replicates). Data are normalized to one of two nontargeting controls.

alongside two nontargeting negative controls and previously validated gRNA targeting the known host and viral dependency factors CXCR4, CYPA, LEDGF, and TSG101 (71, 73). After allowing 4 days for DNA repair, protein depletion, and cell recovery, protein samples were harvested from each polyclonal culture for determination of knockout efficiency. The guide RNA targeting FIP1C displayed varying efficiency, with the multiplexed pool demonstrating near complete knockout, similar to the CYPA control (Fig. 10B). Cell viability was subsequently monitored by staining with a fluorescent amine dye and flow cytometry; no significant differences in cell viability were noted across each knockout population (Fig. 10C).

Given the reported role of FIP1C in Env incorporation, we would not expect to see a replication phenotype in the knockout population until the second round of viral replication. Each knockout population was challenged in technical triplicate with replication-competent, CXCR4-tropic HIV-1 NL4-3 Nef:IRES:GFP. Infection rate (percent green fluorescent protein-positive [GFP⁺] cells) was monitored by flow cytometry at 2 and 5 days postchallenge and normalized to the first nontargeting control (Fig. 10D). At day 2, there was almost no infection of the CXCR4 knockout cells, while infection of the CYPA and LEDGF knockout cells was significantly decreased relative to the nontargeting controls. These differences were even more notable at day 5. The TSG101 knockout cells showed no significant differences from the nontargeting controls at day 2 but had significantly less infection at day 5, consistent with the late-acting phenotype of TSG101. None of the FIP1C knockout cells showed any difference in infection relative to the nontargeting controls at either time point, regardless of gRNA efficiency. To test for the Env dependence of these phenotypes, the same cells were also infected in technical triplicate with single-cycle, VSV-G-pseudotyped, HIV-1 dEnv NL4-3 Nef:IRES:GFP. Infection rate (percent GFP⁺ cells) was monitored by flow cytometry at 2 days postchallenge and normalized to the first nontargeting control (Fig. 10E). As expected, VSV-G pseudotyping rescued infection of the CXCR4 knockout cells, while the CYPA and LEDGF knockout cells showed decreases in infection similar to that of the replication-competent virus at day 2. The FIP1C and TSG101 knockouts had no impact on infection of the single-round virus. Taken together, these data suggest that FIP1C is dispensable for HIV-1 NL4-3 replication in activated, primary CD4⁺ T cells.

DISCUSSION

The function of the long gp41 CT of primate lentiviruses, as well as the identity and role of host factors that interact with the gp41 CT, has long been enigmatic. It is well established that clathrin adapter protein complexes bind the gp41 CT and direct Env internalization from the plasma membrane (4–10). Other factors, including retromer (74), have been demonstrated to interact with the gp41 CT (for a review, see reference 3); however, the role that CT-interacting factors play in Env incorporation and virus propagation remains incompletely understood. To broadly evaluate the role of FIP1C in HIV-1 Env incorporation, particle infectivity, and virus spread, we knocked out FIP1C expression in multiple T-cell lines and primary T cells by using CRISPR-Cas9 technology. We observed a range of phenotypes resulting from *FIP1C* KO. In the Jurkat T-cell line, Env incorporation or virus replication was not reduced. In the SupT1 T-cell line, modest (~41%) reductions in Env incorporation efficiency and single-cycle infectivity were observed, but virus replication kinetics were not affected by *FIP1C* KO. In H9 cells, we observed delayed virus replication, consistent with the results of Qi et al. (60). In this T-cell line, *FIP1C* KO caused an ~36% reduction in Env incorporation efficiency and an overall reduction in Env levels, suggesting that FIP1C KO may reduce the stability of Env in this cell line, perhaps by disrupting Env trafficking. Interestingly, H9 cells expressed more FIP1C protein than SupT1 and were the only cells tested in this study in which FIP1C KO attenuated WT NL4-3 replication. The virus replication defect observed in *FIP1C* KO H9 cells could be rescued by increasing cell density. Because higher cell density and the corresponding increase in cell-cell contacts favor cell-cell virus transmission, these results suggest that the cell-cell mode of HIV-1 spread may be less susceptible to the loss of FIP1C expression than the cell-free mode in H9 cells.

Indeed, cell-cell transfer has been reported to enable HIV-1 to overcome a number of blocks to virus replication (28–32). Perhaps most importantly, *FIP1C* KO did not detectably impair HIV-1 replication in primary CD4⁺ T cells.

We examined Env incorporation and virus replication in two single-cell-derived *FIP1C* KO Jurkat E6.1 clones, designated clones 6 and 9. In clone 6, we observed no significant effect of *FIP1C* KO on Env incorporation, particle infectivity, or virus replication. This result indicates that FIP1C is not required for HIV-1 replication in the Jurkat E6.1 T-cell line. In clone 9, we observed an increase in viral protein (Env and Gag) expression and, correspondingly, more rapid HIV-1 replication kinetics than in parental cells. In our view, considering the results obtained with clone 6, it is unlikely that the increases in viral gene expression and replication kinetics observed with clone 9 were due to the *FIP1C* KO, but rather were probably a property of the single cell from which this clone was derived. These results underscore the importance of analyzing multiple single-cell-derived clones with knockout of a gene of interest or using polyclonal KO cell lines that avoid artifacts stemming from a single-cell origin.

Also underscoring the need to evaluate many cell lines when evaluating novel host factors in viral assembly/replication, in addition to primary T cells, is the finding that many HTLV-1-transformed cells (specifically ED cells) do not express FIP1C. ED cells were not permissive to CTdel144 replication but were permissive to WT HIV-1 replication (data not shown), indicating that they do not behave like MT-4 cells; rather, they behave like non-HTLV-1-transformed T-cell lines in their ability to support HIV-1 replication. Therefore, these data indicate either that FIP1C does not impose a restriction on plasma membrane Env levels or its deficiency is compensated for by a redundant trafficking protein.

As described in the introduction, mutation of the Y₇₉₅W motif in the gp41 CT has been shown to play a role in HIV-1 Env incorporation and particle infectivity (37, 39), and this motif has been implicated in FIP1C-dependent Env incorporation and virus replication (61, 62). The Y₇₉₅W motif was also reported to be required for the Env-dependent relocalization of FIP1C from a perinuclear compartment (potentially a recycling endosome) to the plasma membrane, suggesting that this motif might be required for direct or indirect interactions between the gp41 CT and FIP1C (62).

In this study, we confirmed that the Y₇₉₅W/SL mutation reduces Env incorporation and impairs HIV-1 replication across a range of cell lines. We also demonstrated a role for the highly conserved Tyr residue in this motif in the replication of subtype C HIV-1. However, in our experiments, the defects exhibited by the Y₇₉₅W/SL NL4-3 mutant and the Y₇₉₅S subtype C mutant were independent of FIP1C expression, as similar phenotypes for these mutants were observed in parental and *FIP1C* KO cells. A nuclear magnetic resonance (NMR) solution structure of the gp41 CT embedded in lipid micelles suggested that a region at the N terminus of LLP-3 that is rich in aromatic residues, including Y₇₉₅W, interacts closely with the inner leaflet of the membrane (50). The Y₇₉₅W motif also lies within, and adjacent to, regions of the gp41 CT that have been proposed to interact with MA (37, 51, 75). Mutation of the Y₇₉₅W motif could thus affect the mobility of Env in the membrane, local Env conformation, or interaction of the gp41 CT with the MA domain of Gag, thereby disrupting Env incorporation. Interestingly, Qi et al. (61) reported that the Y₇₉₅W/SL mutant reverted via acquisition of a single amino acid mutation (L₈₅₀/S) near the C terminus of the gp41 CT. It remains to be determined by what mechanism this second-site change rescues the defects exhibited by the Y₇₉₅W/SL mutant.

In summary, the results presented here indicate that while FIP1C appears to play a modest role in Env incorporation in some cell lines, it is not required for HIV-1 replication in most T-cell lines tested or in primary CD4⁺ T cells. Further studies will continue to clarify the role of the enigmatic gp41 CT in HIV-1 replication and its interaction with host cell trafficking machinery.

MATERIALS AND METHODS

Cell lines and tissue culture. HeLa (a gift from P. Spearman), 293T (obtained from the American Type Culture Collection [ATCC]) and TZM-bl (obtained from J. C. Kappes, X. Wu, and Tranzyme, Inc.,

through the NIH AIDS Reagent Program [ARP], Germantown, MD) cell lines were maintained in Dulbecco's modified Eagle medium (DMEM) containing 5% or 10% (vol/vol) fetal bovine serum (FBS), 2 mM glutamine, 100 U/mL penicillin, and 100 μ g/mL streptomycin (Gibco) at 37°C with 5% CO₂. Jurkat E6.1 (64) (catalog no. ARP-177; cell line accession ID on the Cellosaurus database is [CVCL_0367](#)), MT-4 (short tandem repeat [STR] profile in references 64 and 66) (catalog no. ARP-120; Cellosaurus accession ID, [CVCL_2632](#)), C8166-45 (referred to as C8166; Cellosaurus accession ID, [CVCL_0195](#); catalog no. ARP-404), and M8166 (64) (catalog no. ARP-11395; Cellosaurus accession ID, [CVCL_1H07](#)) were obtained from A. Weiss, D. Richman, R. Gallo, and P. Clapham, respectively, through the NIH ARP. The laboratory source of SupT1 used in this study is unknown (64). H9 cells were obtained from R. Gallo (catalog no. ARP-87) through the NIH-ARP and STR profiled to confirm their identity, and they were a 100% match to the Cellosaurus cell line accession ID [CVCL_1240](#). The SupT1-CCR5 (76) (referred to as SupT1huR5; Cellosaurus accession ID, [CVCL_X633](#); STR profile in reference 64) T-cell line was a generous gift from J. Hoxie. The ATL Tax⁻ cells (ED, ATL-55T, and TL-Om1) were a generous gift from C. Giam. T-cell lines were maintained in Roswell Park Memorial Institute (RPMI) 1640 medium containing 10% FBS, 2 mM glutamine, 100 U/mL penicillin, and 100 μ g/mL streptomycin (Gibco) at 37°C with 5% CO₂. Whole blood was obtained from healthy donors via the NCI-Frederick Research Donor Program. hPBMCs were isolated using a Ficoll gradient (Histopaque-1077; Sigma no. 10771), stimulated with 2 μ g/mL phytohemagglutinin P (PHA-P) for 3 to 5 days before infection, and then cultured in 50 U/mL IL-2.

Cloning and plasmids. Unless otherwise indicated, the full-length HIV-1 subtype B molecular clone pNL4-3 was used (77). The Env-deficient pNL4-3/KFS clone, referred to here as Env⁻ (78), and gp41 CT truncation mutant CTdel144 (36) were described previously. The pNL4-3 Y₇₉₅W/SL molecular clone was generated using the QuikChange site-directed mutagenesis kit (Agilent Technologies) on pSL1190-EcoRI-Env WT-XhoI, and cloned into pNL4-3 by EcoRI and XhoI restriction digestion of pSL1190-EcoRI-Env Y₇₉₅W/SL-XhoI and pNL4-3, followed by ligation of the *env* fragment into pNL4-3. The primers were designed to retain the overlapping Rev amino acid sequence. Plasmid sequences were confirmed by restriction digestion with HindIII and Sanger sequencing.

Primers used for mutagenesis were NL4-3 Y₇₉₅W/SL FWD (5'-GGGGTGGGAAGCCCTCAATCCTGTGGAATCTCTAC-3') and NL4-3 Y₇₉₅W/SL REV (5'-GTAGGAGATCCACAAGGATTTGAGGGCTCCACCCC-3'). The full-length HIV-1 transmitted/founder subtype C molecular clones pK3016 (CH185) and pK3058 (CH067) were reported previously (79) and were a gift from C. Ochsenbauer. The pK3016 Y₇₉₅S molecular clone was engineered with the Q5 mutagenesis kit (New England Biolabs) according to the manufacturer's instructions. The primers used did not preserve the overlapping Rev amino acid sequence, but the mutations did not affect viral protein expression, indicating no defect in Rev function. pK3016 and pK3058 were amplified using Stbl3 cells (Thermo Fisher) and standard LB medium. DNA for transfections was purified in large quantities using MaxiPrep kits (Qiagen), and mutations were verified by Sanger sequencing (Macrogen). Plasmid sequences were confirmed by restriction digestion with HindIII and Sanger sequencing of the full plasmid. Primers used for mutagenesis were K3016 Y₇₉₅S FWD (GGGGTGGGAAGCCCTGAAGTCCCTGGGAAGTCTTGTC) and K3016 Y₇₉₅S REV (GCACAAGACTTCCCAGGGACTTCAGGGCTCCACCCC).

siRNA-mediated knockdown of FIP1C. FIP1C knockdown in HeLa cells was accomplished by reverse siRNA transfection. Briefly, 100 pmol of siRNA was diluted in 500 μ L of Opti-MEM in a well of a 6-well plate and gently mixed. Five microliters of Lipofectamine RNAiMax (Thermo Fisher) was added to each well, mixed gently with the siRNA, and incubated for 15 min at room temperature. HeLa cells were diluted in DMEM without serum at a concentration of 2×10^5 cells/mL. Diluted HeLa cells (0.7 mL) were added to the siRNA transfection complex and mixed. The cells were mixed gently and then incubated at 37°C for 4 h. After incubation, 1 mL of DMEM-5% FBS without antibiotics was added to each well. Cells were incubated for 48 h at 37°C and then transfected with pNL4-3 by using Lipofectamine 2000 (Thermo Fisher) according to the manufacturer's instructions. Transfected cells were incubated for 2 days before viral and cell lysates were collected.

Preparation of virus stocks. 293T cells were transfected with HIV-1 proviral DNA using Lipofectamine 2000 (Invitrogen) according to the manufacturer's instructions. Virus-containing supernatants were filtered through a 0.45- μ m membrane 48 h posttransfection, and virus was quantified by measuring RT activity. VSV-G-pseudotyped virus stocks were generated from 293T cells cotransfected with proviral DNA and the VSV-G expression vector pHCMV-G (80) at a DNA ratio of 10:1.

STR profiling and cell line validation. The identity of T-cell lines was confirmed by performing STR profiling as described previously (66). Briefly, genomic DNA was extracted and sent to Genetica (LabCorp) for profiling. The obtained STR profile was compared to the Cellosaurus reference STR using the percent match formula as previously described (64).

Illumina RNA-seq. RNA was extracted from T cells in their exponential growth phase using QIAshredder (Qiagen, catalog no. 79654) and RNeasy Plus minikit (Qiagen, catalog no. 74134). RNA sample integrity was assessed by determining the RNA integrity number (RIN) with an Agilent 2100 Bioanalyzer instrument and applying the eukaryote total RNA Nano assay. RINs were between 9 and 10, indicating intact RNA. Samples were sequenced on a HiSeq 2500, generating an average of 50 million raw reads per sample. Transcript sequence reads were normalized against the total reads for each cell line to generate the number of reads per kilobase per million mapped reads (RPKM). The RPKM is a relative measure of transcript abundance.

Virus replication assays. Virus replication kinetics were determined as previously described (64). Briefly, 2.5×10^6 T cells were transfected with proviral clones (1 μ g DNA/10⁶ cells) in the presence of 700 μ g/mL DEAE-dextran and cultured in 3 mL of RPMI-10% FBS. Every 2 to 3 days, a 200- μ L sample was collected from each flask for the RT assay and frozen in a 96-well plate before the cell cultures were split (Jurkat E6.1, SupT1, SupT1huR5, and H9) 1:3 with fresh medium.

To test the effect of varying cell density on replication kinetics, an equivalent number of cells (2.5×10^6) were transfected with $0.1 \mu\text{g}$ DNA/ 10^6 cells in duplicate and maintained in 5 mL of RPMI–10% FBS. To alter the cell density, one replicate was maintained in a T 25 flask upright (high cell density) and the other replicate was maintained with a T 25 flask lying flat (low cell density).

VSV-G-pseudotyped virus was used to inoculate PHA-stimulated hPBMCs. Virus stocks were normalized by RT activity and used to initiate spreading infection. After 2 h of incubation with VSV-G-pseudotyped virus, cells were washed and resuspended in fresh RPMI–10% FBS plus 50 U recombinant human interleukin 2 (rhIL-2). Every other day, half the medium was replaced without disturbing the cells. Virus replication was monitored by measuring the RT activity in collected supernatants over time. RT activity values were plotted using GraphPad Prism to generate replication curves.

HIV-1 infection of T cells and generation of viral and cell samples for analysis of Env content.

293T cells were plated and cotransfected via lipofectamine 2000 the next day with the pNL4-3 proviral clone and the VSV-G expression vector, pHCMV-G, at a 10:1 ratio. At 48 h posttransfection, supernatants were passed through a $0.45\text{-}\mu\text{m}$ filter and RT activity was measured as described elsewhere (81). T cells were plated the night before transduction in fresh medium at a density of 5×10^6 cells/2 mL. The following day, cells were incubated overnight with RT-normalized virus. The following morning, cells were washed extensively and cultured in 1.5 mL of RPMI–10% FBS. The virus and cell fractions were collected 40 h posttransduction for SupT1huR5 and Jurkat E6.1 cells and 72 h posttransduction for H9 cells. H9 cells were spinoculated for 2 h at 25°C and $200 \times g$ to initiate the transduction, while Jurkat E6.1 and SupT1huR5 cells were not spinoculated.

Virus-containing supernatants were passed through a $0.45\text{-}\mu\text{m}$ filter. A $10\text{-}\mu\text{L}$ portion was set aside for the RT assay, and $200 \mu\text{L}$ was set aside for the TZM-bl infectivity assay. The remaining filtered virus-containing supernatant was layered on a 20% (wt/vol) sucrose–phosphate-buffered saline (PBS) solution and spun for 1.25 h at $100,000 \times g$ at 4°C in a Sorvall S55-A2 fixed-angle rotor (Thermo Fisher Scientific). Cell and virus fractions were solubilized in lysis buffer (30 mM NaCl, 50 mM Tris-HCl [pH 7.5], 0.5% Triton X-100, 10 mM iodoacetamide, complete protease inhibitor [Roche]).

Protein detection. For chemiluminescence-based detection of viral proteins, lysates boiled with $6 \times$ loading buffer (7 mL 0.5 M Tris-HCl–0.4% SDS, 3.8 g glycerol, 1 g SDS, 0.93 g dithiothreitol [DTT], 1.2 mg bromophenol blue) were subjected to SDS-PAGE on 12% 1.5-mm gels and processed using standard Western blotting techniques. All antibodies were diluted in 10 mL of 5% milk in Tris-buffered saline (TBS) blocking buffer. HIV proteins were detected with $10 \mu\text{g}/\text{mL}$ polyclonal HIV immunoglobulin (HIV-Ig) obtained from the NIH ARP. Anti-human IgG conjugated to horseradish peroxidase (HRP; Sigma Aldrich catalog no. GENA933) and used at a 1:5,000 dilution. gp41 was detected with $2 \mu\text{g}/\text{mL}$ 10E8 monoclonal antibody obtained from the NIH ARP (catalog no. 12294) followed by anti-human IgG-HRP as described above. Protein bands were visualized using chemiluminescence with a Bio-Rad universal Hood II ChemiDoc and then analyzed with ImageLab v5.1 software.

For fluorescence-based detection of viral proteins, cell lysates were prepared as described above and loaded on 4 to 15% precast gels (Bio-Rad). After protein separation, proteins were transferred with the Trans-Blot Turbo transfer system (Bio-Rad) according to the manufacturer's instructions using the manufacturer's preset 30 min standard SD protocol onto a low-fluorescence polyvinylidene difluoride (PVDF) membrane (Thermo Fisher). After the transfer, the membrane was blocked for 30 min in 10 mL Azure fluorescent blot blocking buffer (Azure Biosystems). The antibodies 16H3, ches8, and HIV-Ig were diluted 1/5,000 all together in Azure fluorescent blot blocking buffer and 10 mL of the diluted antibodies were added to the membrane. The membrane was incubated with antibodies at 4°C with agitation overnight, washed according to the manufacturer's instructions with Azure fluorescent blot washing buffer (Azure Biosystems) according to the manufacturer's instructions, and incubated with the Azure spectrum fluorescent secondary antibodies goat anti-mouse 800 and goat anti-human 650 at 4°C with agitation overnight. The following day, the membrane was washed extensively with azure fluorescent blot washing buffer, followed by a quick wash with methanol, and then dried in darkness at room temperature. The membrane was then scanned with the Azure Biosystems Sapphire biomolecular imager and analyzed with the Azure spot analysis software.

For detection of cellular proteins, cell lysates were processed as described above and incubated with the following antibodies: anti-GAPDH (1:20,000 dilution; Abcam, catalog no. ab26997), anti- β -actin conjugated directly to HRP (Abcam, catalog no. ab49900), anti-Rab14 (Abcam, catalog no. ab28639), and anti-FIP1C (Cell Signaling, catalog no. 12849). Protein bands were visualized using chemiluminescence with a Bio-Rad universal Hood II ChemiDoc and then analyzed with ImageLab v5.1 software or with the Azure Biosystems Sapphire biomolecular imager and then analyzed with ImageLab v5.1 software or the Azure spot analysis software.

CD4⁺ cell enrichment for FIP1C analysis. Human buffy coats were obtained from healthy volunteers through the NCI-Frederick Research Donor Program. PBMCs were isolated by Ficoll gradient as reported elsewhere (82). CD4⁺ T cells were isolated from PBMCs by magnetic column isolation using the CD4⁺ T-cell isolation kit (Miltenyi Biotec, catalog no. 130-096-533). CD4⁺ cells were also collected.

Single-cycle infectivity assays. TZM-bl infectivity assays were performed as previously described (31). Briefly, 20,000 TZM-bl cells were plated per well in a flat-bottomed, white-walled 96-well plate (Sigma-Aldrich, catalog no. CLS3903-100EA). The following day, the cells were infected with serial dilutions of RT-normalized virus stocks in the presence of $10 \mu\text{g}/\text{mL}$ DEAE-dextran. Approximately 36 h post-infection, cells were lysed with BriteLite luciferase reagent (Perkin-Elmer), and luciferase was measured in a Wallac 1450 Microbeta counter plate reader.

Generation of stable FIP1C KO Jurkat E6.1, SupT1 HuR5, and H9. The LentiCRISPRv2 plasmid, which codes for Cas9 endonuclease and a puromycin resistance selection marker as well as containing a cloning site for single guide RNA (sgRNA) expression, was a gift from Feng Zhang (Addgene, plasmid no.

52961). An sgRNA sequence targeting a site within the first exon of FIP1C was selected by using the CRISPOR design program (83) to identify sgRNAs with high specificity, efficiency, and likelihood of producing out-of-frame indels. The chosen FIP1C sgRNA target sequence was GGGCACGAGCGACGCGTACG. The sgRNA was cloned into LentiCRISPRv2 as previously described (84), to generate the transfer plasmid LentiCRISPRv2-FIP1CsgRNA.

Lentivirus was produced by transfecting HEK293T cells with the LentiCRISPRv2-FIP1CsgRNA transfer plasmid along with the psPAX2 packaging plasmid (gift from Didier Trono; Addgene, plasmid no. 12260) and pVSV-G pseudotyping plasmid (gift from Xuedong Liu, University of Colorado, Boulder, CO), using PEI transfection reagent (no. 43896; Alfa Aesar/Thermo Fisher Scientific, Tewksbury, MA).

Jurkat E6.1, H9, and SupT1huR5 cells were transduced with LentiCRISPRv2-FIP1CsgRNA and selected with 500 ng/mL puromycin beginning 2 days after transduction. After puromycin selection was complete, clonal lines of FIP1C KO Jurkat E6.1 cells were isolated by limiting dilution. FIP1C KO H9 and FIP1C KO SupT1huR5 cells were used without clonal isolation. The polyclonal SupT1 CTRL cell line was generated by transducing an empty LentiCRISPRv2 vector and selecting with puromycin beginning 2 days after transduction for 2 weeks.

CRISPR-Cas9 RNP production, CD4⁺ T cell isolation, and electroporation of primary CD4⁺ T cell cultures. Detailed protocols for RNP production and primary CD4⁺ T cell editing were published previously (72). Briefly, lyophilized CRISPR-Cas9 ribonucleoproteins (crRNA) and transactivating CRISPR RNA (tracrRNA) (Dharmacon) were suspended at a concentration of 160 μ M in 10 mM Tris-HCl (7.4 pH) with 150 mM KCl. Five microliters of 160 μ M crRNA was mixed with 5 μ L of 160 μ M tracrRNA and incubated for 30 min at 37°C. The crRNA-tracrRNA complexes were then mixed gently with 10 μ L of 40 μ M Cas9 (UC-Berkeley Macrolab) to form Cas9 ribonucleoproteins (RNPs). Five 3.5- μ L aliquots were frozen in Lo-Bind 96-well V-bottom plates (E&K Scientific) at -80°C until use. For multiplex RNP synthesis, multiple crRNA targeting the same gene were mixed in equal proportions before proceeding with tracrRNA addition as described above. All crRNAs used in this study were purchased as custom sequences from Dharmacon or derived from the Dharmacon predesigned Edit-R library for gene knockout (see the crRNA sequences below).

Primary human CD4⁺ T cells from healthy donors were isolated from leukoreduction chambers after Trima apheresis (StemCell). PBMCs were isolated by Ficoll centrifugation. Bulk CD4⁺ T cells were subsequently isolated from PBMCs by magnetic negative selection using an EasySep Human CD4⁺ T-cell isolation kit (StemCell; per the manufacturer's instructions). Isolated CD4⁺ T cells were suspended in RPMI 1640 (Sigma) supplemented with 5 mM HEPES (Corning), 50 μ g/mL penicillin-streptomycin (P/S; Corning), 5 mM sodium pyruvate (Corning), and 10% FBS (Gibco). Media were supplemented with 20 IU/ml IL-2 (Miltenyi) immediately before use. For activation, bulk CD4⁺ T cells were immediately plated on anti-CD3-coated plates (coated for 2 h at 37°C with 20 μ g/mL anti-CD3 [UCHT1; Tonbo Biosciences]) in the presence of 5 μ g/mL soluble anti-CD28 (CD28.2; Tonbo Biosciences). Cells were stimulated for 72 h at 37°C and 5% CO₂ prior to electroporation.

Each electroporation reaction mixture consisted of 5×10^5 activated T cells, 3.5 μ L RNPs, and 20 μ L electroporation buffer. After 3 days of stimulation, cells were suspended and counted. RNPs were thawed and allowed to warm to room temperature. Immediately prior to electroporation, cells were centrifuged at $400 \times g$ for 5 min, supernatant was removed by aspiration, and the pellet was resuspended in 20 μ L of room-temperature P3 electroporation buffer (Lonza) per reaction. Twenty microliters of cell suspension was then gently mixed with each RNP and aliquoted into a 96-well electroporation cuvette for nucleofection with the 4D 96-well shuttle unit (Lonza) using pulse code EH-115. Immediately after electroporation, 80 μ L of prewarmed medium with IL-2 was added to each well, and cells were allowed to rest for at least 1 h in a 37°C cell culture incubator. Cells were subsequently moved to 96-well flat-bottomed culture plates prefilled with 100 μ L warm complete medium with IL-2 and anti-CD3-anti-CD2-anti-CD28 beads (T-cell activation and stimulation kit; Miltenyi) at a 1:1 bead-to-cell ratio. Cells were cultured at 37°C and 5% CO₂ in a humidified cell culture incubator for 4 days to allow gene knockout and protein clearance, with additional medium added on day 2. To collect protein lysates for determination of knockout efficiency, 50 μ L of each mixed culture was removed to a centrifuge tube. Cells were pelleted, supernatant was removed, and pellets were resuspended in 75 μ L 2.5 \times Laemmli sample buffer. Protein lysates were heated to 98°C for 20 min before storage at -20°C until immunoblotting.

crRNA sequences. crRNA sequences were obtained from Dharmacon, as follows. For the gene targets named Edit-R crRNA nontargeting control 2 and 3, crRNAs were catalog no. U-007502-20 and U-007503-20 respectively. For the targets CYP4 and TSG101, the crRNAs AGGTCCCAAGACAGCAGGT (catalog no. CM-004979-02) and TTCATTACCTGGGATTGGGA (catalog no. CM-003549-02) were used. Custom sequences were designed for RAB11FIP1: CTCCTCTACAGAGAACCTGG, GGATCTTAAGCAACTGAACC, GGG CACGAGCGACGCGTACG, and TCATCATCACTGTCGACCGA.

Immunoblotting of KO primary CD4⁺ T cell cultures. Samples and PageRuler Plus prestained protein ladder were thawed, and 15 μ L of each was loaded onto 4 to 20% Criterion Tris-HCl SDS-PAGE protein gels (Bio-Rad). Gels were run at 150 V over 90 min until the ladder was sufficiently separated. Proteins were transferred to PVDF membranes by methanol-based electrotransfer (Bio-Rad Criterion blotter) at 90 V for 2 h. Membranes were blocked in 4% milk in PBS-0.1% Tween 20 overnight prior to overnight incubation with primary antibody against CYP4 (clone 79D7; Cell Signaling Technologies), RAB11FIP1 (clone D9D8P; Cell Signaling Technologies) and β -actin (clone 8H10D10; Cell Signaling Technologies) as a protein loading control. Anti-rabbit or anti-mouse immunoglobulin HRP-conjugated secondary antibodies (Bio-Rad) were detected using Hyglo HRP detection reagents (Denville Scientific). Blots were incubated in a 1 \times PBS, 0.2 M glycine, 1.0% SDS, 1.0% Tween 20 (pH 2.2) stripping buffer before reprobing.

Preparation of virus stocks for infection of primary CD4⁺ T cell cultures. Replication-competent reporter virus stocks were generated from an HIV-1 NL4-3 molecular clone in which GFP had been cloned behind an internal ribosomal entry site (IRES) cassette following the viral *nef* gene (NIH AIDS Reagent Program, catalog no. 11349). Briefly, 10 μ g of molecular clone was transfected (PolyJet; SigmaGen) into 5×10^6 HEK293T cells (ATCC CRL-3216) according to the manufacturer's protocol. Twenty-five milliliters of supernatant was collected at 48 and 72 h and combined. Virus-containing supernatant was filtered through 0.45- μ m PVDF filters (Millipore) and precipitated in 8.5% polyethylene glycol (PEG; average M_n , 6,000; Sigma), 0.3 M NaCl for 4 h at 4°C. Supernatants were centrifuged at 3,500 rpm for 20 min, and virus was resuspended in 0.5 mL PBS for a $100\times$ effective concentration. Aliquots were stored at -80°C until use. Single-round reporter virus stocks were generated from a similar HIV-1 NL4-3 dEnv molecular clone with an integrated *nef*-IRES-GFP. Viral particles were pseudotyped with VSV-G by cotransfection with pMD2.G (Addgene catalog co. 12259) at a 3:1 ratio of proviral clone to pMD2.G prior to purification as described above.

HIV-1 infection of primary CD4⁺ T cell cultures. Detailed protocols for HIV-1 spreading infection were described previously (72). Briefly, 6 days postelectroporation, cells were replica plated into triplicate, 96-well, round-bottom plates and cultured overnight in 150 μ L complete RPMI as described above in the presence of 20 IU/mL IL-2. On the following day, 2.5 μ L of concentrated virus stock was added to each well in a 50- μ L carrier volume to bring the total volume in each well to 200 μ L. Cells were cultured in a dark, humidified incubator at 37°C and 5% CO₂. On days 2 and 5 postinfection, 75 μ L of each culture was removed and mixed 1:1 with freshly made 2% formaldehyde in PBS (Sigma) and stored at 4°C for analysis by flow cytometry. Cultures were supplemented with 75 μ L complete, IL-2-containing RPMI medium and returned to the incubator. For single-round infection assays, cells were plated and challenged with 2.5 μ L of single-round, concentrated virus stock as above. Two days postchallenge, 75 μ L of each culture was removed, mixed 1:1 with freshly made 2% formaldehyde in PBS (Sigma), and stored at 4°C for analysis by flow cytometry.

Flow cytometry and analysis of primary CD4⁺ T cell infection data. Flow-cytometric analysis was performed on an Attune NxT acoustic focusing cytometer (Thermo Fisher), recording all events in a 100- μ L sample volume after one 150- μ L mixing cycle. Data were exported as FCS3.0 files and analyzed with a consistent template on FlowJo. Briefly, cells were gated for lymphocytes by light scatter followed by doublet discrimination in both side and forward scatter. Cells with equal fluorescence in the BL-1 (GFP) channel and VL-2 (AmCyan) channel were identified as autofluorescent and excluded from analysis. A consistent gate was then used to quantify the fraction of remaining cells that expressed GFP.

Statistics. Statistics were calculated using GraphPad Prism version 8 for Mac OS (GraphPad Software, La Jolla, CA). Unpaired Student's *t* tests were performed, and two-tailed *P* values of <0.05 , <0.01 , <0.001 , and <0.0001 were considered statistically significant. GraphPad Prism was also used to calculate standard error and to assess statistical significance by one-way analysis of variance (ANOVA). *P* values for Student's *t* test and one-way ANOVA analysis are defined with the same cutoffs.

Ethics statement. PBMCs were obtained from anonymous, deidentified blood donors through the NCI-Frederick Research Donor Program or were purchased through StemCell.

ACKNOWLEDGMENTS

We thank Paul Spearman for providing the HeLa cells used in this study, James Hoxie for providing the SupT1huCCR5 cell line, and Chou-Zen Giam for helpful discussion and for providing the ATL Tax⁻ T cells (ED, ATL-55T, and TL-Om1). We also thank Yongmei Zhao at the NCI Center for Cancer Research Sequencing Facility for performing the Illumina RNA-seq. We thank Christina Ochsenauber for providing the subtype C HIV-1 molecular clones.

This study was supported by the Intramural Research Program of the Center for Cancer Research, National Cancer Institute, NIH, and by an intramural AIDS Research Fellowship (to M.V.F.D.C.). J.F.H. is supported by the Gilead Sciences Research Scholars Program in HIV, NIH/NIGMS funding for the HIV Accessory & Regulatory Complexes (HARC) Center (P50 GM082250), NIH funding for the Third Coast Center for AIDS Research (P30 AI117943), National Health and Medical Research Council Idea Grant 2013215, and NIH/NIAID grants for HIV research (R01 AI150455, R01 AI165236, and R01 AI150998). S.B.V.E. is supported by NIH/NIAID grant for HIV assembly research (R01 AI138625).

M.V.F.D.C. and E.O.F. designed the study, interpreted the data, and wrote the manuscript. M.V.F.D.C., H.K.H., H.C., and L.M.S. performed the experiments. H.K.H. designed the guide RNA targeting FIP1C and generated the lentivector used to generate the SupT1huR5 and H9 FIP1C KO cell lines. H.K.H. also generated the Jurkat E6.1 FIP1C KO clonal cell lines and the H9 FIP1C KO cells. M.V.F.D.C. generated the SupT1huR5 FIP1C knockout cell line and performed all Env incorporation and spreading infection assays. H.C. and L.N. assisted with spreading infection assays. D.A.S. assisted with analysis and interpretation of cell morphology and FIP1C expression and

localization. L.M.S. and J.F.H. performed the virus replication assays in the FIP1C KO primary CD4⁺ T cells. J.F.H. and S.B.V.E. contributed valuable feedback and guidance on CRISPR-Cas9 KO experiments. S.D.A. isolated hPBMCs from human blood and stimulated them for spreading infection assays. L.N. assisted with cell density comparisons in spreading infection assays. All authors contributed to preparation and editing of the manuscript.

All authors declare that they have no competing interests.

REFERENCES

1. Checkley MA, Lutttge BG, Freed EO. 2011. HIV-1 envelope glycoprotein biosynthesis, trafficking, and incorporation. *J Mol Biol* 410:582–608. <https://doi.org/10.1016/j.jmb.2011.04.042>.
2. Postler TS, Desrosiers RC. 2013. The tale of the long tail: the cytoplasmic domain of HIV-1 gp41. *J Virol* 87:2–15. <https://doi.org/10.1128/JVI.02053-12>.
3. Tedbury PR, Freed EO. 2015. The cytoplasmic tail of retroviral envelope glycoproteins. *Prog Mol Biol Transl Sci* 129:253–284. <https://doi.org/10.1016/bs.pmbts.2014.10.009>.
4. Ohno H, Stewart J, Fournier MC, Bosshart H, Rhee I, Miyatake S, Saito T, Gallusser A, Kirchhausen T, Bonifacino JS. 1995. Interaction of tyrosine-based sorting signals with clathrin-associated proteins. *Science* 269:1872–1875. <https://doi.org/10.1126/science.7569928>.
5. Ohno H, Aguilar RC, Fournier MC, Hennecke S, Cosson P, Bonifacino JS. 1997. Interaction of endocytic signals from the HIV-1 envelope glycoprotein complex with members of the adaptor medium chain family. *Virology* 238:305–315. <https://doi.org/10.1006/viro.1997.8839>.
6. Rowell JF, Stanhope PE, Siliciano RF. 1995. Endocytosis of endogenously synthesized HIV-1 envelope protein. Mechanism and role in processing for association with class II MHC. *J Immunol* 155:473–488.
7. Boge M, Wyss S, Bonifacino JS, Thali M. 1998. A membrane-proximal tyrosine-based signal mediates internalization of the HIV-1 envelope glycoprotein via interaction with the AP-2 clathrin adaptor. *J Biol Chem* 273:15773–15778. <https://doi.org/10.1074/jbc.273.25.15773>.
8. Berlioz-Torrent C, Shacklett BL, Erdtmann L, Delamarre L, Bouchaert I, Sonigo P, Dokhelar MC, Benarous R. 1999. Interactions of the cytoplasmic domains of human and simian retroviral transmembrane proteins with components of the clathrin adaptor complexes modulate intracellular and cell surface expression of envelope glycoproteins. *J Virol* 73:1350–1361. <https://doi.org/10.1128/JVI.73.2.1350-1361.1999>.
9. Wyss S, Berlioz-Torrent C, Boge M, Blot G, Honing S, Benarous R, Thali M. 2001. The highly conserved C-terminal dileucine motif in the cytosolic domain of the human immunodeficiency virus type 1 envelope glycoprotein is critical for its association with the AP-1 clathrin adaptor [correction of adapter]. *J Virol* 75:2982–2992. <https://doi.org/10.1128/JVI.75.6.2982-2992.2001>.
10. Byland R, Vance PJ, Hoxie JA, Marsh M. 2007. A conserved dileucine motif mediates clathrin and AP-2-dependent endocytosis of the HIV-1 envelope protein. *Mol Biol Cell* 18:414–425. <https://doi.org/10.1091/mbc.e06-06-0535>.
11. Sauter MM, Pelchen-Matthews A, Bron R, Marsh M, LaBranche CC, Vance PJ, Romano J, Haggarty BS, Hart TK, Lee WM, Hoxie JA. 1996. An internalization signal in the simian immunodeficiency virus transmembrane protein cytoplasmic domain modulates expression of envelope glycoproteins on the cell surface. *J Cell Biol* 132:795–811. <https://doi.org/10.1083/jcb.132.5.795>.
12. Bowers K, Pelchen-Matthews A, Honing S, Vance PJ, Creary L, Haggarty BS, Romano J, Ballensiefen W, Hoxie JA, Marsh M. 2000. The simian immunodeficiency virus envelope glycoprotein contains multiple signals that regulate its cell surface expression and endocytosis. *Traffic* 1:661–674. <https://doi.org/10.1034/j.1600-0854.2000.010810.x>.
13. Bredow B, Arias JF, Heyer LN, Gardner MR, Farzan M, Rakasz EG, Evans DT, Kirchhoff F. 2015. Envelope glycoprotein internalization protects human and simian immunodeficiency virus-infected cells from antibody-dependent cell-mediated cytotoxicity. *J Virol* 89:10648–10655. <https://doi.org/10.1128/JVI.01911-15>.
14. Zhu P, Chertova E, Bess J, Jr, Lifson JD, Arthur LO, Liu J, Taylor KA, Roux KH. 2003. Electron tomography analysis of envelope glycoprotein trimers on HIV and simian immunodeficiency virus virions. *Proc Natl Acad Sci U S A* 100:15812–15817. <https://doi.org/10.1073/pnas.2634931100>.
15. Zhu P, Liu J, Bess J, Jr, Chertova E, Lifson JD, Grise H, Ofek GA, Taylor KA, Roux KH. 2006. Distribution and three-dimensional structure of AIDS virus envelope spikes. *Nature* 441:847–852. <https://doi.org/10.1038/nature04817>.
16. Barria MI, Alvarez RA, Law K, Wolfson DL, Huser T, Chen BK. 2021. Endocytic motif on a biotin-tagged HIV-1 Env modulates the co-transfer of Env and Gag during cell-to-cell transmission. *Viruses* 13:1729. <https://doi.org/10.3390/v13091729>.
17. Wang L, Sandmeyer A, Hubner W, Li H, Huser T, Chen BK. 2021. A Replication-competent HIV clone carrying GFP-Env reveals rapid Env recycling at the HIV-1 T cell virological synapse. *Viruses* 14:38. <https://doi.org/10.3390/v14010038>.
18. Deschambeault J, Lalonde JP, Cervantes-Acosta G, Lodge R, Cohen EA, Lemay G. 1999. Polarized human immunodeficiency virus budding in lymphocytes involves a tyrosine-based signal and favors cell-to-cell viral transmission. *J Virol* 73:5010–5017. <https://doi.org/10.1128/JVI.73.6.5010-5017.1999>.
19. Lodge R, Gottlinger H, Gabuzda D, Cohen EA, Lemay G. 1994. The intracytoplasmic domain of gp41 mediates polarized budding of human immunodeficiency virus type 1 in MDCK cells. *J Virol* 68:4857–4861. <https://doi.org/10.1128/JVI.68.8.4857-4861.1994>.
20. Ball JM, Mulligan MJ, Compans RW. 1997. Basolateral sorting of the HIV type 2 and SIV envelope glycoproteins in polarized epithelial cells: role of the cytoplasmic domain. *AIDS Res Hum Retroviruses* 13:665–675. <https://doi.org/10.1089/aid.1997.13.665>.
21. Owens RJ, Dubay JW, Hunter E, Compans RW. 1991. Human immunodeficiency virus envelope protein determines the site of virus release in polarized epithelial cells. *Proc Natl Acad Sci U S A* 88:3987–3991. <https://doi.org/10.1073/pnas.88.9.3987>.
22. Gardiner JC, Mauer EJ, Sherer NM. 2016. HIV-1 Gag, envelope, and extracellular determinants cooperate to regulate the stability and turnover of virological synapses. *J Virol* 90:6583–6597. <https://doi.org/10.1128/JVI.00600-16>.
23. Dimitrov DS, Willey RL, Sato H, Chang LJ, Blumenthal R, Martin MA. 1993. Quantitation of human immunodeficiency virus type 1 infection kinetics. *J Virol* 67:2182–2190. <https://doi.org/10.1128/JVI.67.4.2182-2190.1993>.
24. Jolly C, Kashefi K, Hollinshead M, Sattentau QJ. 2004. HIV-1 cell to cell transfer across an Env-induced, actin-dependent synapse. *J Exp Med* 199:283–293. <https://doi.org/10.1084/jem.20030648>.
25. Chen P, Hubner W, Spinelli MA, Chen BK. 2007. Predominant mode of human immunodeficiency virus transfer between T cells is mediated by sustained Env-dependent neutralization-resistant virological synapses. *J Virol* 81:12582–12595. <https://doi.org/10.1128/JVI.00381-07>.
26. Iwami S, Takeuchi JS, Nakaoka S, Mammano F, Clavel F, Inaba H, Kobayashi T, Misawa N, Aihara K, Koyanagi Y, Sato K. 2015. Cell-to-cell infection by HIV contributes over half of virus infection. *Elife* 4. <https://doi.org/10.7554/eLife.08150>.
27. Jolly C, Booth NJ, Neil SJ. 2010. Cell-cell spread of human immunodeficiency virus type 1 overcomes tetherin/BST-2-mediated restriction in T cells. *J Virol* 84:12185–12199. <https://doi.org/10.1128/JVI.01447-10>.
28. Sigal A, Kim JT, Balazs AB, Dekel E, Mayo A, Milo R, Baltimore D. 2011. Cell-to-cell spread of HIV permits ongoing replication despite antiretroviral therapy. *Nature* 477:95–98. <https://doi.org/10.1038/nature10347>.
29. Zhong P, Agosto LM, Ilynskaya A, Dorjbal B, Truong R, Derse D, Uchil PD, Heidecker G, Mothes W. 2013. Cell-to-cell transmission can overcome multiple donor and target cell barriers imposed on cell-free HIV. *PLoS One* 8:e53138. <https://doi.org/10.1371/journal.pone.0053138>.
30. Titanji BK, Pillay D, Jolly C. 2017. Combination antiretroviral therapy and cell-cell spread of wild-type and drug-resistant human immunodeficiency virus-1. *J Gen Virol* 98:821–834. <https://doi.org/10.1099/jgv.0.000728>.
31. Van Duyne R, Kuo LS, Pham P, Fujii K, Freed EO. 2019. Mutations in the HIV-1 envelope glycoprotein can broadly rescue blocks at multiple steps in the virus replication cycle. *Proc Natl Acad Sci U S A* 116:9040–9049. <https://doi.org/10.1073/pnas.1820333116>.
32. Hikichi Y, Van Duyne R, Pham P, Groebner JL, Wiegand A, Mellors JW, Kearney MF, Freed EO. 2021. Mechanistic analysis of the broad

- antiretroviral resistance conferred by HIV-1 envelope glycoprotein mutations. *mBio* 12:e13134-20. <https://doi.org/10.1128/mBio.03134-20>.
33. Breed MW, Elser SE, Torben W, Jordan AP, Aye PP, Midkiff C, Schiro F, Sugimoto C, Alvarez-Hernandez X, Blair RV, Somasunderam A, Utay NS, Kuroda MJ, Pahar B, Wiseman RW, O'Connor DH, LaBranche CC, Montefiori DC, Marsh M, Li Y, Piatak M, Jr, Lifson JD, Keele BF, Fultz PN, Lackner AA, Hoxie JA. 2015. Elite control, gut CD4 T cell sparing, and enhanced mucosal T cell responses in Macaca nemestrina infected by a simian immunodeficiency virus lacking a gp41 trafficking motif. *J Virol* 89:10156–10175. <https://doi.org/10.1128/JVI.01134-15>.
 34. Lawrence SP, Elser SE, Torben W, Blair RV, Pahar B, Aye PP, Schiro F, Szeltner D, Doyle-Meyers LA, Haggarty B, Jordan APO, Romano J, Alvarez X, O'Connor DH, Wiseman RW, Fennessey CM, Li Y, Piatak M, Lifson JD, LaBranche CC, Lackner AA, Keele BF, Maness NJ, Marsh M, Hoxie JA. 2021. A tyrosine-based trafficking signal in the simian immunodeficiency virus envelope cytoplasmic domain is strongly selected for in pathogenic SIV infection. *bioRxiv*. <https://doi.org/10.1101/2021.03.31.437834>.
 35. Tedbury PR, Freed EO. 2014. The role of matrix in HIV-1 envelope glycoprotein incorporation. *Trends Microbiol* 22:372–378. <https://doi.org/10.1016/j.tim.2014.04.012>.
 36. Freed EO, Martin MA. 1995. Virion incorporation of envelope glycoproteins with long but not short cytoplasmic tails is blocked by specific, single amino acid substitutions in the human immunodeficiency virus type 1 matrix. *J Virol* 69:1984–1989. <https://doi.org/10.1128/JVI.69.3.1984-1989.1995>.
 37. Murakami T, Freed EO. 2000. The long cytoplasmic tail of gp41 is required in a cell type-dependent manner for HIV-1 envelope glycoprotein incorporation into virions. *Proc Natl Acad Sci U S A* 97:343–348. <https://doi.org/10.1073/pnas.97.1.343>.
 38. Akari H, Fukumori T, Adachi A. 2000. Cell-dependent requirement of human immunodeficiency virus type 1 gp41 cytoplasmic tail for Env incorporation into virions. *J Virol* 74:4891–4893. <https://doi.org/10.1128/jvi.74.10.4891-4893.2000>.
 39. Bhakta SJ, Shang L, Prince JL, Claiborne DT, Hunter E. 2011. Mutagenesis of tyrosine and di-leucine motifs in the HIV-1 envelope cytoplasmic domain results in a loss of Env-mediated fusion and infectivity. *Retrovirology* 8:37. <https://doi.org/10.1186/1742-4690-8-37>.
 40. Day JR, Munk C, Guatelli JC. 2004. The membrane-proximal tyrosine-based sorting signal of human immunodeficiency virus type 1 gp41 is required for optimal viral infectivity. *J Virol* 78:1069–1079. <https://doi.org/10.1128/jvi.78.3.1069-1079.2004>.
 41. Freed EO, Martin MA. 1996. Domains of the human immunodeficiency virus type 1 matrix and gp41 cytoplasmic tail required for envelope incorporation into virions. *J Virol* 70:341–351. <https://doi.org/10.1128/JVI.70.1.341-351.1996>.
 42. Dorfman T, Mammano F, Haseltine WA, Gottlinger HG. 1994. Role of the matrix protein in the virion association of the human immunodeficiency virus type 1 envelope glycoprotein. *J Virol* 68:1689–1696. <https://doi.org/10.1128/JVI.68.3.1689-1696.1994>.
 43. Mammano F, Kondo E, Sodroski J, Bukovsky A, Gottlinger HG. 1995. Rescue of human immunodeficiency virus type 1 matrix protein mutants by envelope glycoproteins with short cytoplasmic domains. *J Virol* 69:3824–3830. <https://doi.org/10.1128/JVI.69.6.3824-3830.1995>.
 44. Tedbury PR, Ablan SD, Freed EO. 2013. Global rescue of defects in HIV-1 envelope glycoprotein incorporation: implications for matrix structure. *PLoS Pathog* 9:e1003739. <https://doi.org/10.1371/journal.ppat.1003739>.
 45. Murphy RE, Saad JS. 2020. The interplay between HIV-1 Gag binding to the plasma membrane and Env incorporation. *Viruses* 12:548. <https://doi.org/10.3390/v12050548>.
 46. Tedbury PR, Novikova M, Ablan SD, Freed EO. 2016. Biochemical evidence of a role for matrix trimerization in HIV-1 envelope glycoprotein incorporation. *Proc Natl Acad Sci U S A* 113:E182–E190. <https://doi.org/10.1073/pnas.1516618113>.
 47. Tedbury PR, Novikova M, Alfidhli A, Hikichi Y, Kagiampakis I, KewalRamani VN, Barklis E, Freed EO. 2019. HIV-1 matrix trimerization-impaired mutants are rescued by matrix substitutions that enhance envelope glycoprotein incorporation. *J Virol* 94:e01526-19. <https://doi.org/10.1128/JVI.01526-19>.
 48. Alfidhli A, Barklis RL, Barklis E. 2009. HIV-1 matrix organizes as a hexamer of trimers on membranes containing phosphatidylinositol-(4,5)-bisphosphate. *Virology* 387:466–472. <https://doi.org/10.1016/j.virol.2009.02.048>.
 49. Qu K, Ke Z, Zila V, Anders-Osswein M, Glass B, Mucksch F, Muller R, Schultz C, Muller B, Krausslich HG, Briggs JAG. 2021. Maturation of the matrix and viral membrane of HIV-1. *Science* 373:700–704. <https://doi.org/10.1126/science.abe6821>.
 50. Murphy RE, Samal AB, Vlach J, Saad JS. 2017. Solution structure and membrane interaction of the cytoplasmic tail of HIV-1 gp41 protein. *Structure* 25:1708–1718.E5. <https://doi.org/10.1016/j.str.2017.09.010>.
 51. Piai A, Dev J, Fu Q, Chou JJ. 2017. Stability and water accessibility of the trimeric membrane anchors of the HIV-1 envelope spikes. *J Am Chem Soc* 139:18432–18435. <https://doi.org/10.1021/jacs.7b09352>.
 52. Pezeshkian N, Groves NS, van Engelenburg SB. 2019. Single-molecule imaging of HIV-1 envelope glycoprotein dynamics and Gag lattice association exposes determinants responsible for virus incorporation. *Proc Natl Acad Sci U S A* 116:25269–25277. <https://doi.org/10.1073/pnas.1910008116>.
 53. Goud B, Liu S, Storrie B. 2018. Rab proteins as major determinants of the Golgi complex structure. *Small GTPases* 9:66–75. <https://doi.org/10.1080/21541248.2017.1384087>.
 54. Borchers AC, Langemeyer L, Ungermann C. 2021. Who's in control? Principles of Rab GTPase activation in endolysosomal membrane trafficking and beyond. *J Cell Biol* 220. <https://doi.org/10.1083/jcb.202105120>.
 55. Pfeffer SR. 2013. Rab GTPase regulation of membrane identity. *Curr Opin Cell Biol* 25:414–419. <https://doi.org/10.1016/j.cob.2013.04.002>.
 56. Gillingham AK, Sinka R, Torres IL, Lilley KS, Munro S. 2014. Toward a comprehensive map of the effectors of rab GTPases. *Dev Cell* 31:358–373. <https://doi.org/10.1016/j.devcel.2014.10.007>.
 57. Thomas LL, Fromme JC. 2020. Extensive GTPase crosstalk regulates Golgi trafficking and maturation. *Curr Opin Cell Biol* 65:1–7. <https://doi.org/10.1016/j.cob.2020.01.014>.
 58. Hales CM, Griner R, Hobdy-Henderson KC, Dorn MC, Hardy D, Kumar R, Navarre J, Chan EK, Lapierre LA, Goldenring JR. 2001. Identification and characterization of a family of Rab11-interacting proteins. *J Biol Chem* 276:39067–39075. <https://doi.org/10.1074/jbc.M104831200>.
 59. Horgan CP, McCaffrey MW. 2009. The dynamic Rab11-FIPs. *Biochem Soc Trans* 37:1032–1036. <https://doi.org/10.1042/BST0371032>.
 60. Qi M, Williams JA, Chu H, Chen X, Wang JJ, Ding L, Akhrome E, Wen X, Lapierre LA, Goldenring JR, Spearman P. 2013. Rab11-FIP1C and Rab14 direct plasma membrane sorting and particle incorporation of the HIV-1 envelope glycoprotein complex. *PLoS Pathog* 9:e1003278. <https://doi.org/10.1371/journal.ppat.1003278>.
 61. Qi M, Chu H, Chen X, Choi J, Wen X, Hammonds J, Ding L, Hunter E, Spearman P. 2015. A tyrosine-based motif in the HIV-1 envelope glycoprotein tail mediates cell-type- and Rab11-FIP1C-dependent incorporation into virions. *Proc Natl Acad Sci U S A* 112:7575–7580. <https://doi.org/10.1073/pnas.1504174112>.
 62. Kirschman J, Qi M, Ding L, Hammonds J, Dienger-Stambaugh K, Wang JJ, Lapierre LA, Goldenring JR, Spearman P. 2018. HIV-1 envelope glycoprotein trafficking through the endosomal recycling compartment is required for particle incorporation. *J Virol* 92:e01893-17. <https://doi.org/10.1128/JVI.01893-17>.
 63. Emerson V, Haller C, Pfeiffer T, Fackler OT, Bosch V. 2010. Role of the C-terminal domain of the HIV-1 glycoprotein in cell-to-cell viral transmission between T lymphocytes. *Retrovirology* 7:43. <https://doi.org/10.1186/1742-4690-7-43>.
 64. Fernandez MV, Hoffman HK, Pezeshkian N, Tedbury PR, van Engelenburg SB, Freed EO. 2020. Elucidating the basis for permissivity of the MT-4 T-cell line to replication of an HIV-1 mutant lacking the gp41 cytoplasmic tail. *J Virol* 94:e01334-20. <https://doi.org/10.1128/JVI.01334-20>.
 65. Staubus AO, Alfidhli A, Barklis RL, Barklis E. 2019. Replication of HIV-1 envelope protein cytoplasmic domain variants in permissive and restrictive cells. *Virology* 538:1–10. <https://doi.org/10.1016/j.virol.2019.09.008>.
 66. Fernandez MV, Delviks-Frankenberry KA, Scheiblin DA, Happel C, Pathak VK, Freed EO. 2019. Authentication analysis of MT-4 cells distributed by the National Institutes of Health AIDS Reagent Program. *J Virol* 93:e01390-19. <https://doi.org/10.1128/JVI.01390-19>.
 67. Miyoshi I. 1982. Type C-virus producing cell lines derived from adult T cell leukemia. *GANN Monogr Cancer Res* 28:219–228.
 68. Jeang KT, Darse D, Matocha M, Sharma O. 1997. Expression status of Tax protein in human T-cell leukemia virus type 1-transformed MT4 cells: recall of MT4 cells distributed by the NIH AIDS Research and Reference Reagent Program. *J Virol* 71:6277–6278. <https://doi.org/10.1128/JVI.71.9.6277-6278.1997>.
 69. Oguariri RM, Dai L, Adelsberger JW, Rupert A, Stevens R, Yang J, Huang D, Lempicki RA, Zhou M, Baseler MW, Lane HC, Imamichi T. 2013. Interleukin-2 inhibits HIV-1 replication in some human T cell lymphotropic virus-1-infected cell lines via the induction and incorporation of APOBEC3G into the virion. *J Biol Chem* 288:17812–17822. <https://doi.org/10.1074/jbc.M113.468975>.

70. LANL. HIV sequence database. AnalyzeAlign. https://www.hiv.lanl.gov/content/sequence/ANALYZEALIGN/analyze_align.html. Accessed 5 January 2021.
71. Hultquist JF, Schumann K, Woo JM, Manganaro L, McGregor MJ, Doudna J, Simon V, Krogan NJ, Marson A. 2016. A Cas9 ribonucleoprotein platform for functional genetic studies of HIV-host interactions in primary human T cells. *Cell Rep* 17:1438–1452. <https://doi.org/10.1016/j.celrep.2016.09.080>.
72. Hultquist JF, Hiatt J, Schumann K, McGregor MJ, Roth TL, Haas P, Doudna JA, Marson A, Krogan NJ. 2019. CRISPR-Cas9 genome engineering of primary CD4(+) T cells for the interrogation of HIV-host factor interactions. *Nat Protoc* 14:1–27. <https://doi.org/10.1038/s41596-018-0069-7>.
73. Selyutina A, Persaud M, Simons LM, Bulnes-Ramos A, Buffone C, Martinez-Lopez A, Scoca V, Di Nunzio F, Hiatt J, Marson A, Krogan NJ, Hultquist JF, Diaz-Griffero F. 2020. Cyclophilin A prevents HIV-1 restriction in lymphocytes by blocking human TRIM5alpha binding to the viral core. *Cell Rep* 30:3766–3777.E6. <https://doi.org/10.1016/j.celrep.2020.02.100>.
74. Groppelli E, Len AC, Granger LA, Jolly C. 2014. Retromer regulates HIV-1 envelope glycoprotein trafficking and incorporation into virions. *PLoS Pathog* 10:e1004518. <https://doi.org/10.1371/journal.ppat.1004518>.
75. Alfadhli A, Staubus AO, Tedbury PR, Novikova M, Freed EO, Barklis E. 2019. Analysis of HIV-1 matrix-envelope cytoplasmic tail interactions. *J Virol* 93:e01079-19. <https://doi.org/10.1128/JVI.01079-19>.
76. Means RE, Matthews T, Hoxie JA, Malim MH, Kodama T, Desrosiers RC. 2001. Ability of the V3 loop of simian immunodeficiency virus to serve as a target for antibody-mediated neutralization: correlation of neutralization sensitivity, growth in macrophages, and decreased dependence on CD4. *J Virol* 75:3903–3915. <https://doi.org/10.1128/JVI.75.8.3903-3915.2001>.
77. Adachi A, Gendelman HE, Koenig S, Folks T, Willey R, Rabson A, Martin MA. 1986. Production of acquired immunodeficiency syndrome-associated retrovirus in human and nonhuman cells transfected with an infectious molecular clone. *J Virol* 59:284–291. <https://doi.org/10.1128/JVI.59.2.284-291.1986>.
78. Freed EO, Delwart EL, Buchschacher GL, Jr, Panganiban AT. 1992. A mutation in the human immunodeficiency virus type 1 transmembrane glycoprotein gp41 dominantly interferes with fusion and infectivity. *Proc Natl Acad Sci U S A* 89:70–74. <https://doi.org/10.1073/pnas.89.1.70>.
79. Parrish NF, Gao F, Li H, Giorgi EE, Barbian HJ, Parrish EH, Zajic L, Iyer SS, Decker JM, Kumar A, Hora B, Berg A, Cai F, Hopper J, Denny TN, Ding H, Ochsenbauer C, Kappes JC, Galimidi RP, West AP, Jr, Bjorkman PJ, Wilen CB, Doms RW, O'Brien M, Bhardwaj N, Borrow P, Haynes BF, Muldoon M, Theiler JP, Korber B, Shaw GM, Hahn BH. 2013. Phenotypic properties of transmitted founder HIV-1. *Proc Natl Acad Sci U S A* 110:6626–6633. <https://doi.org/10.1073/pnas.1304288110>.
80. Yee JK, Friedmann T, Burns JC. 1994. Generation of high-titer pseudotyped retroviral vectors with very broad host range. *Methods Cell Biol* 43:99–112. [https://doi.org/10.1016/S0091-679X\(08\)60600-7](https://doi.org/10.1016/S0091-679X(08)60600-7).
81. Freed EO, Martin MA. 1994. Evidence for a functional interaction between the V1/V2 and C4 domains of human immunodeficiency virus type 1 envelope glycoprotein gp120. *J Virol* 68:2503–2512. <https://doi.org/10.1128/JVI.68.4.2503-2512.1994>.
82. Sabado RL, Miller E, Spadaccia M, Vengco I, Hasan F, Bhardwaj N. 2013. Preparation of tumor antigen-loaded mature dendritic cells for immunotherapy. *J Vis Exp* 2013:50085. <https://doi.org/10.3791/50085>.
83. Haeussler M, Schonig K, Eckert H, Eschstruth A, Mianne J, Renaud JB, Schneider-Maunoury S, Shkumatava A, Teboul L, Kent J, Joly JS, Concordet JP. 2016. Evaluation of off-target and on-target scoring algorithms and integration into the guide RNA selection tool CRISPOR. *Genome Biol* 17:148. <https://doi.org/10.1186/s13059-016-1012-2>.
84. Sanjana NE, Shalem O, Zhang F. 2014. Improved vectors and genome-wide libraries for CRISPR screening. *Nat Methods* 11:783–784. <https://doi.org/10.1038/nmeth.3047>.